Data in brief: Conceptual design-optimisation of futuristic hydrogen powered ultrahigh bypass ratio geared turbofan engine

Swapnil S. Jagtap [a*], Peter R.N. Childs [b] and Marc E.J. Stettler [a]

[a] Centre for Transport Studies, Department of Civil and Environmental Engineering, Imperial College London, London SW7 2AZ, United Kingdom

[b] Energy Futures Lab, Imperial College London, London SW7 2AZ, United Kingdom

* Corresponding author: swapniljagtap111@gmail.com

Abstract:

This is additional data to the main paper publication

Link to the main paper:

https://www.sciencedirect.com/science/article/abs/pii/S036031992404535X

Nomenclature

AR	Aspect ratio
BCC	Braided carbon composite
BPR	Bypass ratio
BWB	Blended wing body
CMC	Ceramic matric composites
c_p	Specific heat capacity
C_p	Molar heat capacity at constant pressure
C_v	Molar heat capacity at constant volume
FAR	Fuel-air ratio
FC	Fuel consumption
FPR	Fan pressure ratio
GTF	Geared turbofan
GTOW	Gross take-off weight
HPC	High pressure compressor
HPT	High pressure turbine
IGV	Inlet guide vane
IPC	Intermediate pressure compressor
ISA	International standard atmosphere
L/D	Lift to drag ratio
LDI	Lean direct injection
LH_2	Liquid hydrogen
LHV	Lower heating value
LPP	Lean Premixed Pre-vapourised
LPT	Low pressure turbine
LTA	Large twin aisle
nmi	Nautical mile
NO_x	Oxides of nitrogen
OEM	Original equipment manufacturers
OEW	Operating empty weight
OPR	Overall pressure ratio
P_3	Total pressure at combustor inlet
PFR	Plug flow reactor
PMC/Al honeycomb	Polymer matrix composite-aluminium honeycomb core
R’	Universal gas constant
RQL	Rich-burn Quick-quench Lean-burn
RR	Rate of reaction
SiC	Silicon carbide
SLS	Sea level static
S_L^o	Laminar premixed flame speeds
SPK	Synthetic paraffin kerosene
Ti-6Al-4V	Titanium alloy
TET	Turbine entry temperature
TOC	Top of climb
TSEC	Thrust specific energy consumption
TSFC	Thrust specific fuel consumption
T/W	Thrust to weight ratio
T_2	Fan inlet temperature
T_3	Total temperature at combustor inlet
T_4	Turbine entry temperature
UHB	Ultra-high bypass ratio
VLTA	Very large twin aisle
$W_{F,block}$	Block fuel weight
$W_{F,total}$	Total fuel weight carried at mission start
WSR	Well-stirred reactor
α	Diffusive transport of energy (and species) from reaction zone into unburned gases
Φ	Equivalence ratio

SI 1. Literature Review

SI 1.1 Review of aircraft and engine design process

In the current section, the approaches for the gas turbine engine design and aircraft design process are reviewed, as both processes are very important towards the research goals. This section reviews the design approaches used for aircraft performance modelling. It is imperative to first understand and get familiarised with the practiced process of gas turbine engine design and aircraft design. These processes are first studied in detail and based on the published approaches individual models are developed in the respective paper parts considering the research scope.

SI 1.1.1 Aircraft design process

The aircraft design process can be categorised into three main phases: conceptual, preliminary, and detailed design according to Raymer [1], Sadraey [2], Fielding [3], Kirby [4], Torenbeek [5], and Kundu et al. [6], and this is represented in Figure SI 1 in the form of a schematic. Original equipment manufacturers (OEMs) have differing approaches to aircraft design and so Figure SI 1 represents an aggregate of some commonly used methods.

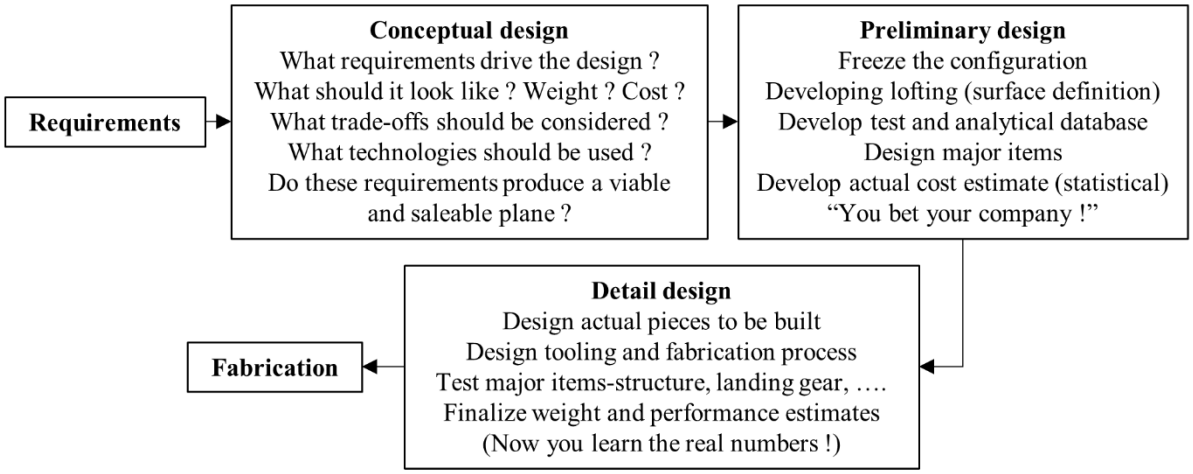

Figure SI 1. Phases of aircraft design process (source [1])

SI 1.1.1.1 Conceptual design

Following the schematic indicated in Figure SI 1, designers would consider and examine a wide range of aircraft architecture concepts, perform trade studies of the designs and the requirements, and then finalise a best design, and with significant customer input, finalise a well-balanced list of requirements. The conceptual design stage is a fluid process, and it answers the fundamental questions of configuration arrangement, weight and size, and performance. The customer requirements are addressed in this step, and sometimes the customer may wish to relax the requirements. As a design is assessed in increasing detail, novel ideas and problems emerge. Every time the recent design is evaluated and sized, it must be updated and re-sketched to reflect the latest parameters such as gross weight, wing size, fuel

weight, engine size, and other updates. Early wind-tunnel experiments frequently reveal problems requiring some modifications to the configuration [1]–[6].

SI 1.1.1.2 Preliminary design

Preliminary design may start when the major modifications are completed, and important design questions have been resolved. In this stage, the finalised concept from the previous stage is refined and studied in sufficient detail. The configuration/arrangement can be anticipated to remain similar to the current drawings, but minor revisions may occur. In later stages of preliminary design, even minor modifications are stopped after it is decided to freeze the configuration. During this stage, the specialists in areas such as control systems, structures, etc. will design and investigate their section of the aircraft. Testing begins in the areas like structures, propulsion, aerodynamics, and stability and control. A mock-up may be manufactured at this stage. A crucial activity during this design stage is 'lofting', which is the mathematical modelling of the outer skin (or airframe) of the aircraft with sufficient accuracy. This ensures proper fit of different components, even if they are designed and manufactured by different designers in various locations. The ultimate purpose of preliminary design is to prepare the company for the next step i.e., the detail design stage, which is also referred to as full-scale development. Therefore, the completion of preliminary design usually comprises of a full-scale development proposal. Preliminary design should establish a confidence that the aircraft can be manufactured on time and at the estimated cost [1]–[6].

SI 1.1.1.3 Detail design

With a favourable decision for entering a full-scale development, the detail design phase is started. It comprises of designing the actual components and their sub-components in detail, which will be fabricated. Another crucial step in the detail design is called as production design, where the specialists determine how the aircraft will be fabricated. This begins with the simplest and smallest assemblies of sub-components and then building up to the final assembly process. The production designers often wish to change the design considering the aspect of manufacturing ease, which may have a significant impact on the weight and/or performance. Minor modifications are unavoidable, but the design should meet the original requirements. During this design stage, the testing efforts intensifies. The actual aircraft structure is manufactured and tested. The control laws for the flight control system are tested. These tests are conducted on a detailed working model of the flight control surfaces and actuators. Both company and customer test-pilots fly on the developed flight simulators. This design stage ends with aircraft manufacturing [1]–[6].

SI 1.1.2 Aircraft engine design process

In general, the engine design process comprises of three stages: conceptual, preliminary and detailed design [7]–[9]. Figure SI 2 from NASA's 'A manual for preliminary design of gas turbine engines, volume I: Overview', depicts this design process and is reported by Hendricks [7]. As can be observed from Figure SI 2, the level of detail to the engine definition in each phase, increases from phase 1 to 3. In Figure SI 2, FPR, BPR, and OPR are the engine fan pressure ratio, bypass ratio, and overall pressure ratio, respectively. The entire engine design

process is only conducted completely by the engine manufacturers. Every engine manufacturer has their individual perspective of this overall process, which is a well-guarded industry secret for gaining a competitive advantage over their rival manufacturers. Therefore, it is difficult to state an exact layout of the industry used engine design process. However, different authors with extensive industrial experience have published their perspective of the overall engine design process [8]–[10].

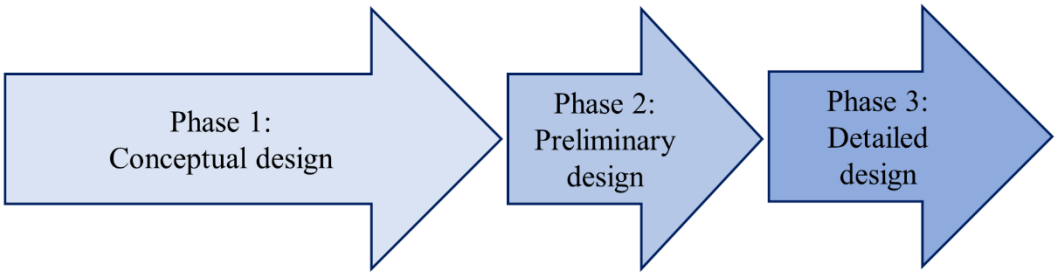

Known	• Basic mission requirements • Duty cycle • Material limits (thermal, mechanical, cost)		• Aero-elastic requirements • Fatigue requirements • Flutter requirements • Overall strength requirements	• Local strength requirements • Producibility • Functional requirements
Results	Thermodynamic cycle • BPR • OPR • FPR • Pressure and temperature • Airflow	Design objectives • Performance • Weight goals • Cost goals	• Flow-path geometry • Weights • Major loads, stresses, deflections	• Detail design - Mechanisms - Joints, attachments • Production drawings

Figure SI 2. Aircraft engine design process (data source [7])

Books on gas turbine engine design by Saravanamuttoo et al. [10], Mattingly [8], and Walsh and Fletcher [9], provide their engine design schematic. Consideration of off-design performance in the engine design is important for the engine to meet the performance requirements at all off-design points in the flight mission. The engine design schematic by Saravanamuttoo et al. [10] identifies a critical engine design path in the engine design process and it excludes the off-design performance from this critical path. Saravanamuttoo et al. [10] state that the off-design analysis can be conducted separately from the critical design path. This limits the ability to effectively meet the performance requirements at off-design points. Therefore, only the engine design schematics by Mattingly [8] (discussed below), and Walsh and Fletcher [9] (discussed in SI §1.2) are considered in this work which consider the off-design process towards an effective engine design.

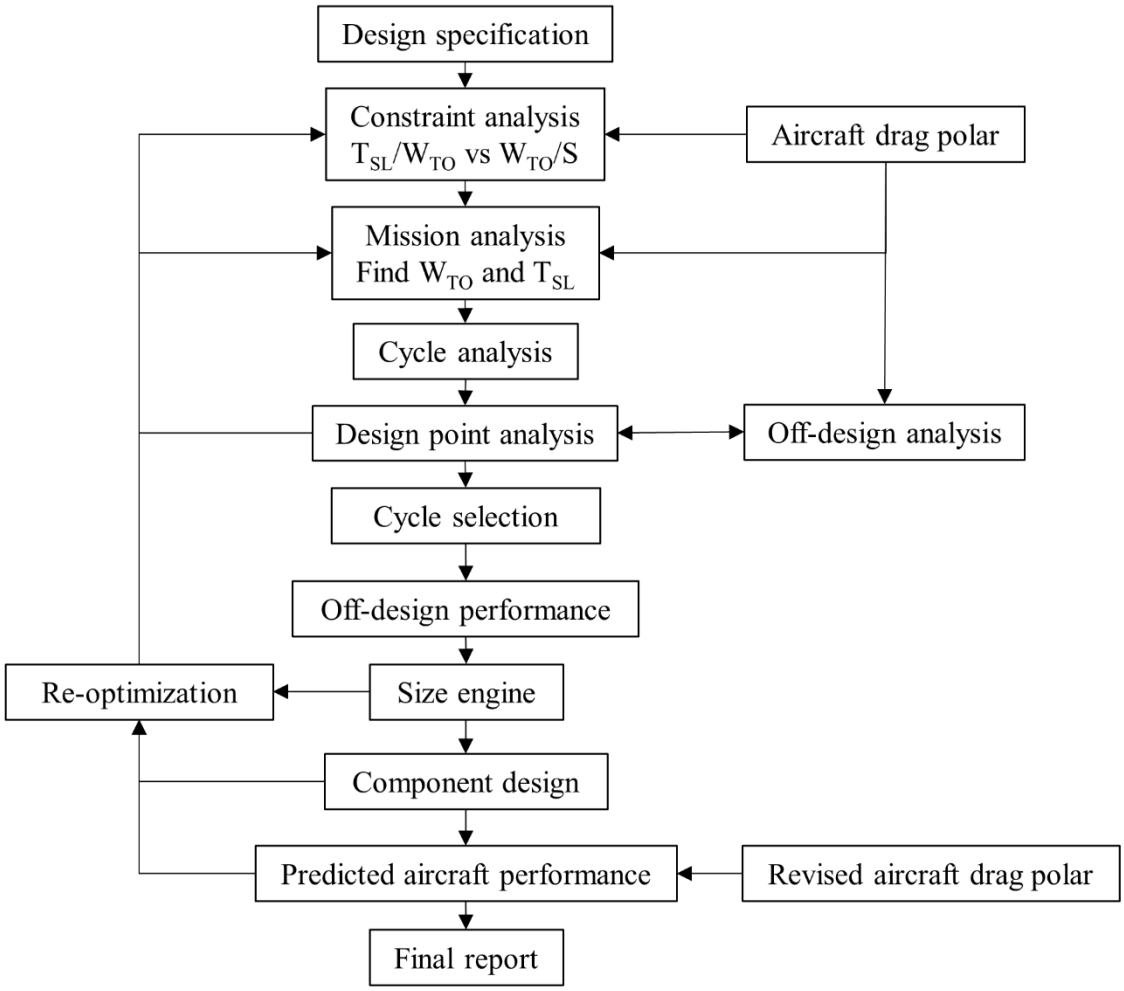

Figure SI 3. Preliminary propulsion design sequence (data source [8])

Mattingly [8] presents a preliminary propulsion design sequence which is depicted in Figure SI 3. This sequence provides the engine design process within the context of the overall aircraft design process. Thus, it starts with determining the aircraft specifications and associated drag polar, and thereafter conducting the constraint and mission analysis. When the process ends, the engine design is used to evaluate the performance of the aircraft, which can potentially result in a return to the mission analysis for performing iteration(s) of the engine design. This sequence comprises of design point or on-design analysis, and off-design analysis. After selecting the engine cycle and evaluating the entire off-design performance envelope, the size of engine and design of components is conducted. The component design is thus conducted before the end of the process and requires iteration(s) when the performance does not meet the assumptions made in prior steps.

SI 1.2 Review of aircraft engine conceptual design process

It is imperative to first understand and get familiarised with the practiced process of conceptual aircraft engine design, before developing an engine model using this design approach. This process is first studied in detail and based on the published approaches a model is developed.

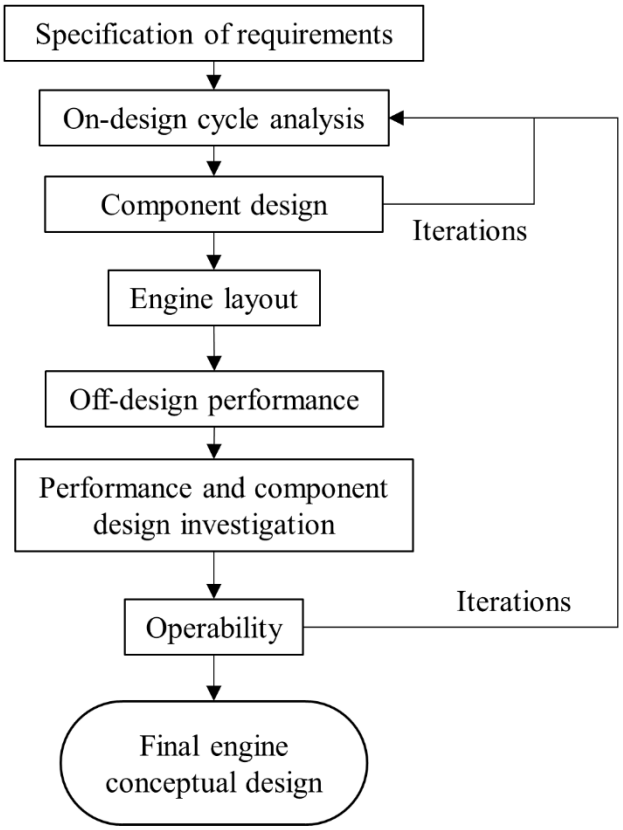

Figure SI 4. Aircraft engine conceptual design process (source [7])

Walsh and Fletcher [9] discuss the engine design steps focussed on the conceptual design stage. This is synthesised and reported by Hendricks [7] as a schematic, and is shown in Figure SI 4. This schematic is useful in defining the boundaries of the conceptual engine design process, which is the scope of the present work. In general, these steps are similar to those presented by Mattingly [8] (as seen in Figure SI 3). However, the order of the design steps, is different. The on-design cycle analysis and component design are the steps considered earlier in the process by Walsh and Fletcher [9]. The off-design assessment of both the cycle and component performance come at a later stage in the process. An extra step to examine the engine operability is included in the scheme, for which the author mentions that this step is frequently skipped. The are many iteration loops identified which should be executed when the cycle and component performance do not match, or when the overall engine performance does not match the constraints and requirements.

The engine design and optimisation scheme used in this work is along the lines of the schematic of Walsh and Fletcher [9] shown in Figure SI 4 as it is more holistic and specific to the conceptual engine design phase as compared to the engine design schematic of Mattingly [8].

SI 1.3 Hydrogen powered gas turbine engine

SI 1.3.1 Hydrogen combustion mechanism

Hydrogen is a promising alternative aviation fuel because of its high gravimetric energy density of 120 MJ/kg compared to 43.2 MJ/kg of conventional jet fuel (kerosene/Jet-A) [11].

There are other aspects in terms of combustion physics that must be considered for the use of hydrogen as a fuel in gas turbine engines. There is a need to first understand few relevant terms and mechanisms before proceeding with the analysis of the fuel switch from Jet-A to hydrogen in gas turbine engines.

Primarily, it is important to understand the respective combustion chemistry/chemical reaction mechanism of Jet-A-air and hydrogen-air combustion. The equivalence ratio (Φ) is defined as the ratio of actual fuel-air ratio (FAR) and the stoichiometric FAR and is represented by equation SI 1. Φ is given by,

$$\Phi = \frac{FAR_{actual}}{FAR_{stoichiometric}} \tag{SI 1}$$

$$\text{where } FAR_{stoichiometric} = \frac{Molecular\ weight_{fuel}}{a'\left(1+\frac{0.79}{0.21}\right) Molecular\ weight_{air}}. \tag{SI 2}$$

A 'major combustion species' model is presented below in equation SI 3 (source [12]), which provides a generic combustion reaction of fuel C_xH_y with typical major products of combustion. It is given by,

$$C_xH_y + a\left(O_2 + \frac{0.79}{0.21} N_2\right) \rightarrow \text{b } CO_2 + c\ CO + d\ H_2O + e\ H_2 + fO_2 + \frac{0.79}{0.21} a\ N_2 \tag{SI 3}$$

For fuel lean and stoichiometric condition i.e. $\Phi \leq 1$, equation SI 3 transforms to equation SI 4 (source [12]) as the reactant mixture is air rich and there will not be excess fuel to produce CO (c = 0) and H_2 (e = 0), as the combustion products, and this is represented by,

$$C_xH_y + a\left(O_2 + \frac{0.79}{0.21} N_2\right) \rightarrow \text{b } CO_2 + d\ H_2O + fO_2 + \frac{0.79}{0.21} a\ N_2 \tag{SI 4}$$

Similarly, for fuel rich conditions i.e. $\Phi>1$, equation SI 3 transforms to equation SI 5 (source [12]) as the reactant mixture is fuel rich and there will not be excess oxidizer (especially oxygen, as nitrogen is considered to stay unreacted in this simple major species model) left over by the end of the combustion process. Thus,

$$C_xH_y + a\left(O_2 + \frac{0.79}{0.21} N_2\right) \rightarrow \text{b } CO_2 + c\ CO + d\ H_2O + e\ H_2 + \frac{0.79}{0.21} a\ N_2 \tag{SI 5}$$

Future aircraft combustors are expected to burn leaner than present combustors because of improved efficiency as a result of high overall pressure ratio and bypass ratios [13]. Henceforth, in this work for all analytical purposes, only equation SI 4 is useful and relevant. The composition of air used in the equations below is 79% nitrogen and 21% oxygen, which is used for simplicity and is a theoretical composition typically used for analytical purposes. The resulting molecular weight of air is 28.85 g/mol. However, the composition of air is slightly different than the theoretical composition. In reality, air additionally includes other inert and non-inert gases resulting in a molecular weight of air of 28.97 g/mol [14]–[16]. The coefficients in equation SI 4 are a, b, d, and f, are represented by equation SI 6 and these are given by,

$$a = \frac{x + \frac{y}{4}}{\Phi} \; ; b = x \; ; d = \frac{y}{2} \; and \; f = \frac{(1 - \Phi)}{\Phi}\left(x + \frac{y}{4}\right) \tag{SI 6}$$

Knowing the actual FAR, Φ can be calculated using equations SI 1, SI 2, and SI 6 for a given fuel-air combination. In this work, the actual FAR is predicted by GasTurb 13 [17] for both conventional jet fuel and hydrogen fuel. Jet-A fuel/kerosene is represented by the molecular formula of $C_{11.6}H_{22}$ (molecular weight of 161.5 g/mol) [18]. Therefore, x is 11.6 and y is 22 in equations SI 2 to SI 6. The combustion equation for Jet-A fuel for Φ <1 is represented by equation SI 7, and this is assumed to also apply to 100% synthetic paraffin kerosene (SPK). The resulting equation SI 7 is arranged for 1 mole of air in the reactant, and is given by,

$$\frac{0.21\Phi}{17.1} C_{11.6}H_{22} + (0.21O_2 + 0.79N_2) \rightarrow \frac{2.436\Phi}{17.1} CO_2 + \frac{2.31\,\Phi}{17.1} H_2O + 0.21(1 - \Phi)\, O_2 + 0.79\, N_2 \tag{SI 7}$$

Similarly, for H_2, x = 0 and y = 2 equations SI 2 to SI 6, thereby b = 0. Therefore, the combustion equation for hydrogen fuel for Φ < 1 is represented by equation SI 8, which is arranged for 1 mole of air in the reactant, and this is represented by,

$$0.42\Phi\, H_2 + (0.21\, O_2 + 0.79\, N_2) \rightarrow 0.42\Phi\, H_2O + 0.21(1 - \Phi)O_2 + 0.79\, N_2 \tag{SI 8}$$

Therefore, if the Φ is known, the mass and molecular weight of both reactants and products can be calculated, for both Jet-A and hydrogen (mass is conserved). Both equations SI 7 and SI 8 are highly simplified because these do not include typical minor species like NO, NO_2, OH, etc. However, from analytical viewpoint both equations SI 7 and SI 8, are very helpful to predict mass and molecular weight of products. These equations are used in the results section (in SI §5) for estimating the product mass and molecular weight of the products of combustion. This is very helpful in understanding the energy efficiency improvement in hydrogen engines, especially for same thrust production as that of Jet-A engine, where actual fuel to air ratio is known. The molecular weight of products of combustion of gas turbine engines powered by Jet-A/kerosene is similar to the molecular weight of air, in the typical regime of engine operation [16], [19].

The reaction rate of hydrogen is seven times as that of conventional jet fuel [13]. This significant difference between the reaction rates of the two fuels can be analytically explained from fundamental sciences. From kinetic theory of gases, the root mean squared speed, most probable speed, and mean speed of gas is inversely related to its the molar mass [20]. Comparing the properties of hydrogen (molecular weight of 2 g/mol) and kerosene (molecular weight of 161.5 g/mol), it is clear that the molar mass of the former case is significantly lower. This results in high speeds of hydrogen molecules. Rate of a reaction can be understood from kinetic theory of gases through the molecular collision frequency [21]. Collision frequency is proportional to the speed of gases [20]. Therefore, because of significantly higher speeds of hydrogen gas relative to kerosene (heavier molecule), the rate of reaction is higher for hydrogen compared to kerosene. Another simple reasoning for the seven times higher rate of reaction of

hydrogen compared to kerosene is the significant difference in the number of bonds to be broken during combustion. Kerosene which is typically represented by $C_{11.6}H_{22}$, is a heavier hydrocarbon (molecular weight of 161.5 g/mol) which has multiple bonds, compared to H_2 (molecular weight of 2 g/mol). Due to the significantly lower number of bonds to be broken during the combustion of H_2, compared to kerosene, hydrogen has a higher rate of reaction.

The comparison of laminar premixed flame speeds (S_L^o) between different fuels can be done using equation SI 9 (source [22]), and it is given by,

$$S_L^o \propto \sqrt{\alpha\, \mathrm{RR}} \tag{SI 9}$$

where α is the diffusive transport of energy (and species) from reaction zone into unburned gases and RR is the rate of reaction. Hydrogen is lighter compared to kerosene, and therefore it can diffuse quickly or has higher diffusion relative to kerosene. Additionally, as discussed above, the rate of reaction of hydrogen is seven times higher than kerosene. Therefore, as per equation SI 9 the flame speed of hydrogen is greater than that for kerosene.

For a flow channel (like a tube), if the diameter is smaller than some critical value, then the flame will not propagate in the tube even if the gas velocity in the tube is lower than the adiabatic flame speed. This critical diameter value is called as the quenching diameter which can be inversely scaled with the flame speed for analytical purpose [23]. Therefore, the quenching diameter for hydrogen (higher flame speed) is lower than that of kerosene. Flashback is an uncontrolled propagation of the flame upstream of combustion chamber because of a local imbalance in the flame speed and flow velocity [12]. If hydrogen is used directly in the gas turbine engines with same fuel lines designed for Jet-A then hydrogen will flash-back with flame propagation that can reach the fuel tank. Therefore, fuel systems must be designed that establish reliability and redundancy.

SI 1.3.2 Engine operational issue for hydrogen use

During engine start, hydrogen travels from the cryogenic tanks through the fuel lines to the combustor. Before this, the fuel lines are void of hydrogen and only air present there. With the presence of ambient air in the fuel lines there is a high risk of combustion at the moment when hydrogen interacts with air [24]. This could potentially lead to flash back during the engine start-up phase [the previously discussed aspect of (critical) quenching diameter for hydrogen fuel lines is relevant here]. This risk can be eliminated by purging the fuel lines with an inert gas. Nitrogen can be used as a cheap substitute for an inert gas. Additionally, there is a possibility of solidification of gases when they encounter cryogenic hydrogen which can impede fuel flow. The purging of fuel lines will also be necessary while shutting down the engine.

Hydrogen not only has a high energy density per unit mass but is also an excellent heat sink (can be used to cool components). The cooling capacity of hydrogen is about 4.9 times the cooling capacity of conventional jet fuel and approximately 2.8 times the cooling capacity of CH_4 [24]. Before the fuel enters the combustion chamber it should be preheated. This ensures that the fuel has completely vapourised during the condition maximum flow rate from the cryogenic tank. This can be safely and effectively performed by using a heat exchanger. Installation of fuel lines in the vicinity of engine hot sections is not recommended because any

fuel leak will immediately result in high flammability risk. The use of a separate fluid in a heat exchanger will cool the hot sections of the engine, where the cryogenic hydrogen cools this separate fluid in the heat exchanger and in the process, hydrogen starts warming. Cooling the hot engine sections will help in the reduction of energy needed for combustion. This further ensures that the fuel will be fully in a gaseous state before injection. This increases component life and thermal efficiency, while benefiting from the heat sink potential of cryogenic hydrogen (as discussed above). Engine starting will need an electrical heater that increases the fuel temperature and after the engine reaches its idle rotational speed the heat exchanger becomes fully functional. Furthermore, a metering system is needed to be installed, as it can regulate the required liquid and gas fuel flow rate for different power settings.

SI 1.3.3 Hydrogen powered combustors

Hydrogen combustion in gas turbine engines is more complex than just a simple FAR modification. It also depends on the geometry of combustor [25]. The addition of hydrogen to conventional fuels improves engine performance though the performance of using 100% hydrogen in conventional combustors is inferior to conventional fuels [24]. This drop in the performance is because of combustors geometry being insufficient for the effective mixing of air and fuel. As discussed in SI §1.3.1, the flame speed of hydrogen is greater than kerosene, where the conventional combustors are designed for the flame speeds of kerosene. Hydrogen combustion in conventional combustor result in large diffusive flames where stoichiometric ratios are found in the flame vicinity. This causes very high temperatures and resultantly high oxides of nitrogen (NO_x) emissions. These issues can be resolved by considering all flame attributes of combustion like combustion efficiency, flame stability, acoustics, and other crucial diagnostics, for the design of a hydrogen fired combustor. After considering these aspects, two novel combustor concepts have emerged through research-development, for the effective and efficient combustion of hydrogen such that its full potential can be used. The two concepts of hydrogen combustors that are likely to be future alternatives are: the lean direct injection (LDI) examined by Marek et al. [13]; and the Micro-mix concepts studied by Dahl and Suttrop [26]. These two designs have proven to be successful via actual combustion experiments. Both design/concepts are similar in their methodology. Both concepts establish that flashback is a primary concern with the desire of increasing fuel mixing [24]. In both designs, the hydrogen-air mixing strength is significantly enhanced for preventing the formation of large diffusion flames that result in higher NO_x emissions. By improving the mixing strength, the flame length reduces for desired combustion quality, with lower combustor residence time. NO_x depends on residence time and temperature. Enhancing the strength of mixing (or reducing the residence time) will result in very low NO_x emissions. The two concepts of hydrogen combustors are discussed as follows:

LDI combustor:

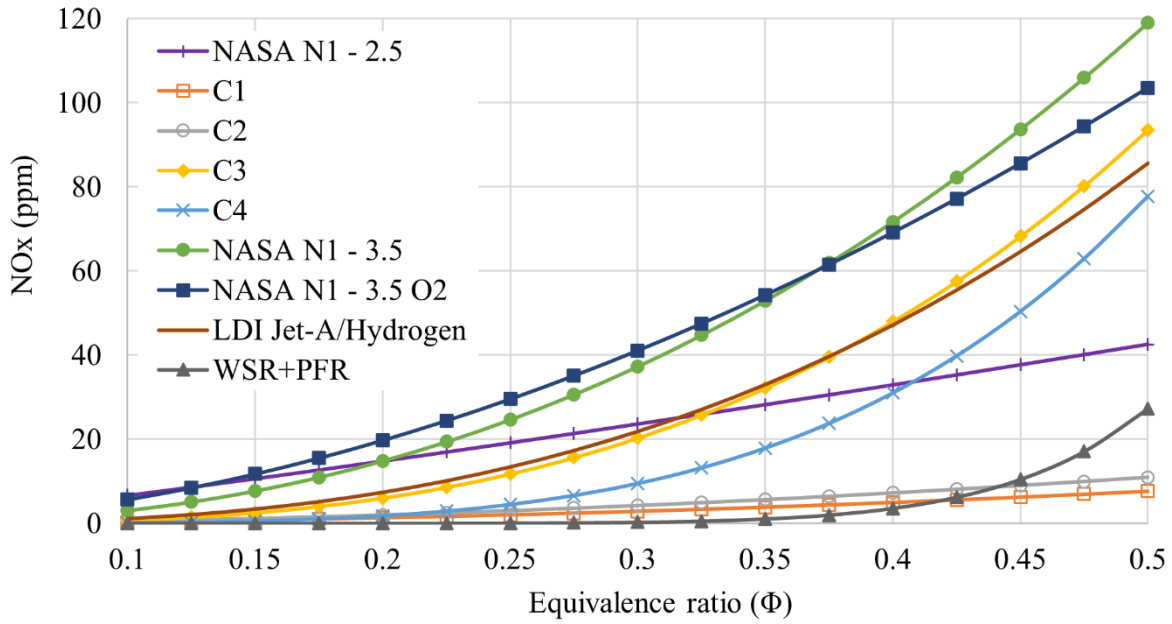

Figure SI 5. Comparison of NO_x emission (ppm) for different LDI combustor configurations at combustor inlet temperature of 700 K, combustor inlet pressure of 6.8 atm., 4% fuel injector air flow pressure drop and 2 milliseconds of combustor residence time (created using correlations from Marek et al. [13])

Multiple configurations/types of LDI combustors were studied by Marek et al. [13] at NASA's Glenn research centre, which is capable of replicating typical conditions of gas turbine engine operations and ensuring reliability. In the combustor, flashback is prevented by using a H_2 inlet tube of size lower than the quenching diameter for hydrogen. Marek et al. find that the performance of hydrogen LDI combustors is outstanding as compared with the performance of advanced Jet-A LDI combustors. Different configurations of fuel injectors are studied in the LDI experiments by Marek et al. (the injector and combustor geometry details can be found in [13]). Figure SI 5 provides a comparison of NO_x emission (ppm) for different LDI combustor configurations at combustor inlet temperature of 700 K, combustor inlet pressure of 6.8 atm., 4% fuel injector air flow pressure drop and 2 milliseconds of combustor residence time (using correlations from Marek et al.).

Referring to Figure SI 5, using injector C3 produces similar NO_x emissions compared to LDI Jet-A, but it is an injector design that is simple, durable, and safe. The design of injector C4 is similar to the design of injector C3 but its NO_x emissions are lower for equivalence ratios below 0.4 (or combustor temperature lower than 1,650 K). Injector C4 is durable and there is considerable radial mixing. C1 and C2 configurations have best performance in terms of NO_x emission reductions, both of which produce less than half of NO_x produced by LDI Jet-A combustor. The C1 injector failed during the experiments and therefore it could not be examined completely over the desired pressure range. C2 is unique in design, and it encourages very fast mixing. However, the durability and cooling of C2 was compromised as it resulted into a failure. All LDI examinations by Marek et al. are very stable. The LDI combustors result in reduced NO_x levels without any auto-ignition or flashback. Other combustor (computational)

configuration like a well-stirred reactor (WSR) followed by a plug flow reactor (PFR), practically produce near-zero NO_x at equivalence ratios below 0.325, and it releases lower NO_x than C1 and C2 at equivalence ratios below 0.425.

Micro-mix combustor:

The micro-mix combustor is studied by Dahl and Suttrop [26] for hydrogen combustion. The study demonstrates safe combustion of hydrogen with focused efforts on minimising the NO_x production. The objective of the study by Dahl and Suttrop was to convert the auxiliary power unit (APU) of A320 i.e., GTCP 36-300, such that it safely functions on hydrogen. The hydrogen combustor is designed using miniaturised diffusive combustion. This type of combustion improves the local mixing regions. Miniaturised diffusive combustion prevents the large diffusive flames (very high temperature zones) observed in hydrogen combustion conducted in conventional combustor. The enhanced mixing is a result of turbulence formations and the breakdown of eddies, which decreases the residence times, and the stoichiometric conditions are prevented.

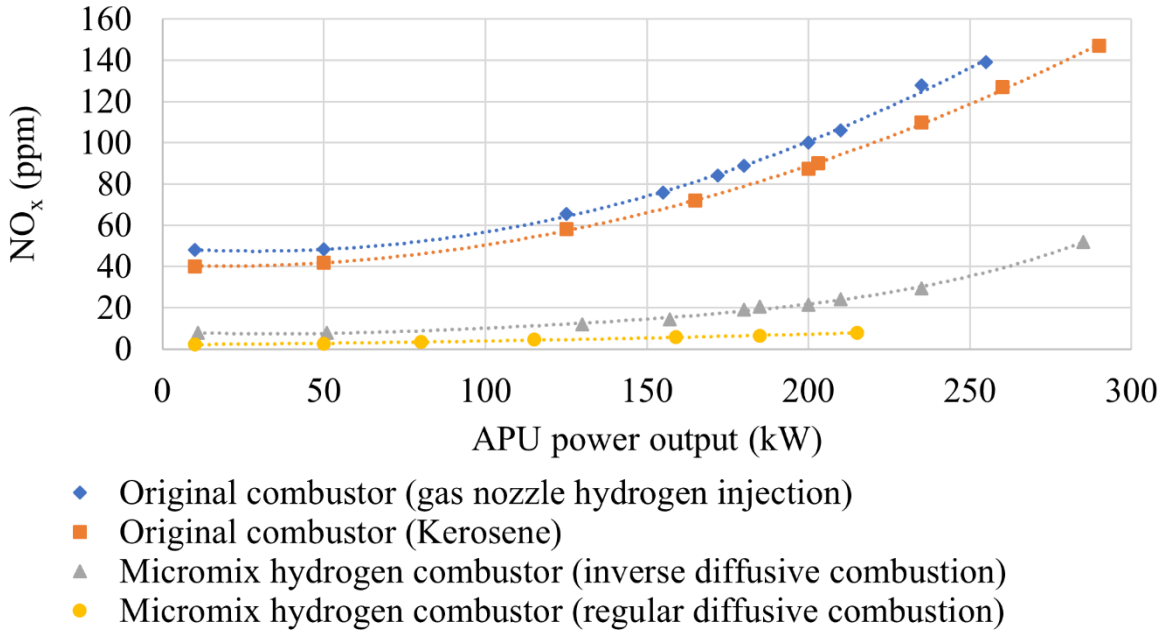

Figure SI 6. Comparison of NO_x emissions performance of APU powered by conventional jet fuel and hydrogen fuel in conventional combustor and micro-mix combustor (data source [24], [26]**)**

Figure SI 6 shows the NO_x emissions performance comparison of APU powered by conventional jet fuel and hydrogen fuel in conventional combustor and micro-mix combustor (data source [24], [26]). The highest NO_x emissions are found in hydrogen combustion using conventional combustor, because of the large diffusive flames that tend to be at the stoichiometric conditions. High temperatures occur at stoichiometric conditions and NO_x emission production is temperature dependent. The use of micro-mix combustor for hydrogen combustion produces lowest NO_x emissions because it principally prevents stoichiometric conditions through improvement in local mixing strength.

SI 1.4 GasTurb

The design and optimisation of the ultra-high bypass ratio (UHB) geared turbofan (GTF) engine will be conducted using commercial software called GasTurb 13 [17]. An overview of the GasTurb 13 software is provided below.

SI 1.4.1 On-design point calculation

During the design process of the gas turbine engine, a thermodynamic cycle will be calculated and selected for the on-design point [17], [27]–[29]. The total temperatures, total pressures, and mass flows, at the entry and exit of all engine components are calculated. The Mach numbers and hub-tip ratios for the components determine the crucial engine dimensions considering the aero-thermodynamics. Thus, through the selection/calculation of the cycle design point (on-design point), the flow-annulus geometry and the engine weight are determined. In addition to the engine geometry, the disk stresses are calculated.

At this point in GasTurb 13, the flow annulus geometry, turbine and compressors disks, and engine cross section, are designed. Thus, as compared to pure zero-dimensional/cycle analysis, more details on engine simulation are known and the quality of the design analysis is improved significantly. Additionally, more insights are obtained on the interaction between component aerodynamics, thermodynamics, and the mechanical design of gas turbine engines.

SI 1.4.2 Off-design point calculation

At off-design points, the performance of a gas turbine engine with a given/fixed geometry (from the on-design point) is evaluated. During the initiation of an off-design point analysis, the component design points should be correlated with the component maps. This can be conducted automatically via standard GasTurb maps and the standard design point settings in these maps. The maps are scaled (by GasTurb) to size at the initiation of the off-design point calculations in such a manner that the maps are consistent with the on-design point [17], [27]–[29].

SI 1.4.3 Standard maps

For every turbine and compressor there is one standard map [17], [27]–[29]. These maps are taken from open literature for axial flow turbomachinery, and these are physically sound depiction of real turbomachines.

SI 1.4.4 Selected maps

The accuracy of the off-design estimation is dependent on the validity of the component maps on whether or not they reflect the component performance [17], [27]–[29]. The selected maps have a catalogue of pre-selected maps which provide numerous and different maps for different components, where each of them depicts a common turbine or compressor design. This enables the selection of the most suitable component maps and resultantly improving the accuracy of the off-design performance.

SI 1.4.5 Cycle optimisation algorithms

In GasTurb 13, any cycle output parameter can be chosen as an objective function or figure of merit which can be minimised or maximised [17], [27]–[29]. There are different optimisation algorithm/process available in GasTurb: random new start search, adaptive random search, endless random search, and systematic search. Whichever strategy is used initially for the optimisation should be complemented with other search strategies for ensuring that the estimated optimum point is global and not local. The 'random new start' will initiate a random search by shifting away from the previous optimum point towards the estimation of the new optimum. In the 'adaptive random search' algorithm, random numbers are used for the optimisation variables which are concentrated in the vicinity of the best prior optimum. The systematic search strategy is a gradient based search. The best optimum point estimated during all searches is the final outcome of an endless random search. The endless random search is ideal for cases where there are numerous optimisation variables and constraints, making the optimisation problem more complex. If the similar optimum point is obtained using multiple strategies, then it is clear that the point is the global optimum.

SI 1.4.6 Disk design and optimisation

During the off-design mode, information such as engine geometry and the disk stress at any operational point can be obtained, however, the engine geometry cannot be modified [17], [27]–[29]. Disk design and optimisation can be conducted in the off-design mode.

After the engine performance analysis, the disk dimensions and the disk stress should be analysed at both on- and off-design points, such that the disks are not overstressed at any operating point. GasTurb recommends that the disks should be optimised one by one, via several optimisation attempts for every disk. The optimisation should be initiated from different disk-shape points. During the disk optimisation, both the systematic search and random search should be used.

SI 2. Design requirements and known data

SI 2.1 Future engine and aircraft design data from literature

The design characteristics of the long-range NASA N+2 blended wing body (BWB) GTF aircraft and Boeing 777-200LR (datum used by NASA), for 301 passengers are listed in Table SI 1. Additionally, the engine data of NASA N+2 BWB 301-GTF aircraft is provided in Table SI 2. Based on the information in Table SI 1 and Table SI 2, design targets are set for the engine. The graphical representation of this NASA N+2 BWB 301-GTF aircraft configuration can be found in resource [30].

Table SI 1. NASA N+2 BWB 301-GTF and B777-200LR aircraft data (source [30])

Characteristics	Value
Boeing 777-200LR	
Block fuel consumption	125,706 kg
NASA's N+2 BWB 301-GTF aircraft	
Range	7,500 nautical-miles (nmi) or 13,890 km
Passengers	301
Powerplant	2 geared turbofan engines
Fuel type	Conventional jet fuel
Cruise Mach	0.84
Gross take-off weight (GTOW)	242,441 kg
Operating empty weight (OEW)	114,907 kg
Payload weight	53,570 kg
Wingspan	76.2 m
Wing area	944.73 m^2
Aspect ratio (AR)	6.1
Total fuel at mission start	73,965 kg
Block fuel consumption	66,683 kg
Saving in block fuel consumption relative to B777-200LR	47%

Table SI 2. Engine data of NASA N+2 BWB 301-GTF aircraft (source [30])

Parameters	Units	Top of climb (TOC)	Sea Level Static (SLS)
Mach and altitude	- , m	0.8 at 10,668 m	0, 0 m
Net thrust	kN	55.603	299.9
Specific fuel consumption	g/kN-s	13.15	5.62
OPR	-	60.0	47.1
BPR	-	17.65	20
FPR	-	1.35	1.25
Bare engine weight	kg	6,789.37	
Accessories weight	kg	835.06	
Engine mount weight	kg	137.44	
Total engine weight	kg	7,761.87	
Nacelle and inlet weight	kg	776.15	
Fan diameter		132.4 inches or 3.36296 m	
Power off-take	kW	150	
Bleed		Zero	

SI 2.2 Specification of requirements

The design requirement/specification is a necessary step for initiating the design process which can be observed from Figures SI 1 to SI 4. In the current work, the design requirement is to conduct a conceptual design of a large twin aisle (LTA) BWB aircraft for transporting 301 passengers over a range of 7,500 nmi or 13,890 km. This aircraft should be

powered by (liquid hydrogen) LH_2 for zero direct-carbon emissions (operational phase) and 100% SPK, separately. For developing designs of LH_2 aircraft and 100% SPK aircraft, a baseline case is required where this BWB aircraft is powered by Jet-A. Modifications to the baseline case are made for the use of LH_2 fuel and 100% SPK (separately), where the modifications are based on published literature. The aircraft design requirements are listed in Table SI 3, and these are based on Table SI 1. It is to be noted that the GTOW and OEW from Table SI 1 are not listed in Table SI 3 because these are expected to change since the engine weight might change because of use of next generation lighter materials. For uniformity with the NASA N+2 BWB aircraft study [30] (reference study), the ratio of block fuel weight ($W_{F,block}$) to the total fuel weight carried at mission start ($W_{F,total}$) is kept unchanged for modelling the use of Jet-A, LH_2 fuel, and 100% SPK. For the BWB Jet-A (baseline) case, except for the engine weights, there is no other change expected. In case of LH_2 fuel, modifications are required to the aircraft which changes the total aircraft weight.

Table SI 3. Aircraft design requirements

Characteristics	Value
Range	7,500 nautical-miles (nmi) or 13,890 km
Passengers	301
Powerplant	Two geared turbofan engines
Fuel type	1. Conventional jet fuel 2. Liquid hydrogen (LH_2) 3. 100% SPK
Cruise Mach and altitude	0.84 at 10,668 m (35,000 ft)
Payload weight	53,570 kg
Wingspan	76.2 m
Wing area	944.73 m^2
Aspect ratio	6.1
Total conventional jet fuel at mission start	73,965 kg

Table SI 4. Engine design requirements

Parameters	Units	TOC	SLS
Mach and altitude	- , m	0.8 at 10,668 m	0, 0 m
Net thrust	kN	55.603	299.9
OPR	-	60.0	47.1
BPR	-	17.65	20
FPR	-	1.35	1.25
Fan diameter*		132.4 inches or 3.36296 m	
Power off-take	kW	150	
Bleed	-	Zero	
Drive and engine type	-	Geared turbofan engine	

* is a design requirement only for baseline (BWB Jet-A) case, LH_2 case 1, and 100% SPK

For 100% SPK, slight modifications are required to the baseline aircraft for accommodating a slightly less dense fuel (as learnt from [31]) which changes the OEW and GTOW.

In the context of engine design, which is the scope of this work, the design requirements are listed in Table SI 4. The listed parameters in Table SI 4 are set as design requirement since the NASA N+2 BWB aircraft has been assessed for noise assessment. It is assessed at 40.3 effective perceived noise levels in decibels (EPNLdB) cumulative 'below' the Stage 4 certification level. The parameters in Table SI 4 viz. thrust (exhaust velocity), FPR (with fan diameter), significantly contribute to noise emission. The OPR changes as FPR changes, and therefore is considered as a design requirement here. The high engine BPR can be perceived as a technology metric which has an impact on noise emission reduction.

SI 2.3 Data for engine design

Considering the design requirements set above, a discussion is required on the data known from literature. This data comprises of engine design and technology used currently and planned to be used in the future, which can be useful for meeting the set engine design requirements. The objective of this work is to design a UHB GTF engine that meets the requirements listed in Table SI 4. The engine data in terms of component efficiencies, stage count, advanced materials, cooling flows, and combustor technology, are discussed as follows. These form the basis of most inputs to the engine model developed in this work.

SI 2.3.1 Component efficiencies

Table SI 5. Engine component efficiencies presently (source [17])

Component		Value (%)
Fan	Inner	91.00
	Outer	90.37
Intermediate pressure compressor (IPC)		92.01
High pressure compressor (HPC)		91.00
High pressure turbine (HPT)		89.00
Low pressure turbine (LPT)		92.16

Table SI 6. Future engine component efficiencies

Component		SLS [32]	TOC [32]	Cruise [32]	Climb
		(in %)			
Fan	Inner Outer	92.1	92.8	94.4	94.1
IPC		92.6	92.5	93.0	92.2
HPC		92.1	91.2	93.0	92.8
HPT		93.6	94.4	93.5	94.4
LPT		94.1	95.6	93.8	95.6

The engine design and optimisation will be conducted using commercial software called as GasTurb 13 [17]. Table SI 5 and Table SI 6 list gas turbine engine's component efficiencies for the present and future technology, respectively. In Table SI 5 the component efficiencies are taken from GasTurb 13 [17] and in Table SI 6 component efficiencies for all operating point except 'climb' come from NASA's study [32] for the H3.2 aircraft. The H3.2 aircraft is a BWB aircraft having propulsion systems installed aft of the aircraft, similar to the aircraft design requirement set in this work. The component efficiencies during climb in Table SI 6 is calculated by taking an average of respective component efficiencies at take-off and top-of-climb for the H3.2 aircraft from NASA's study [32].

SI 2.3.2 Turbomachinery stage count

The stage count of the turbomachinery in a gas turbine engine is an important aspect. Depending on the turbomachinery stage-loading, the distribution of work between stages of this machine is determined. Therefore, for a fixed engine geometry, if a compressor with standard stage loading is used to do the required work, but with lower stage count, then the compressor might not be able to conduct the required compression, as it isn't designed for these conditions. On the other hand, if more stages of a turbomachinery are selected, then it can increase the engine weight. Therefore, selection of turbo-machinery stage count is very crucial.

In this work, the selection of stage counts for compressor and turbines is based on three studies: Kestner et al. [33], Bijewitz et al. [34], and Pratt and Whitney's GTF engine PW1100G [35]. The engine compression system includes IPC and HPC, and expansion system includes HPT and LPT. Kestner et al. [33] and Bijewitz et al. [34] design turbofan engines for future applications. Table SI 7 lists the stage count of compressor and turbines from the three studies. It also provides the stage counts used in this work. It can be observed from Table SI 7 that the stage counts between the three studies are very similar except the stage counts for the HPC and LPT.

Kestner et al. [33] use stage count of 10 for the HPC citing the GEnx engine (used on the latest Boeing 787 aircraft), which has same number of stages. PW1100G engine [35] has a stage count of 8 for the HPC. Bijewitz et al. [34] arrives at a value of stage count of 9 for the HPC based on trade studies that take into consideration stage loading and feasible stage pressure ratios. Moreover, the design parameters of the study by Bijewitz et al. [34] is almost similar to the current work. Therefore, stage count of 9, similar to the study by Bijewitz et al. [34], for the HPC is selected here.

Table SI 7. Stage counts of engine compressors and turbines

Component	Stage count			
	Kestner et al. [33]	Bijewitz et al. [34]	PW 1100 G [35]	Present work
Fan	1	1	1	1
IPC	3	3	3	3
HPC	10	9	8	9
HPT	2	2	2	2
LPT	3	4	3	3

In case of LPT stage count, the value of 3 is selected, similar to the study by Kestner et al. [33] and to the PW1100G engine [35]. Firstly, it is observed in the methodology section of the main paper that the gear ratio is one of the optimisation design variables. Gear ratio is linked to the low-pressure spool speed. The low-pressure spool speed along with the stage loading determine the stage count. Secondly, low pressure turbines are large components compared to the high-pressure systems, hence have more weight. Considering both these points, especially the weight aspect, stage count of 3 similar to the study by Kestner et al. [33] and to the PW1100G engine [35], is used here for LPT.

SI 2.3.3 Engine materials

Most advanced materials (with advanced component manufacturing process) that are planned to be used in future aircraft engines are currently expensive. Therefore, use of these materials is cost prohibitive currently. The use of these materials provides benefits during the engine operation. The examples of these benefits are engine weight reduction due to use of lighter materials, high operating temperatures due to the use of ceramic matric composites (CMC), implementation of materials with excellent strength for reducing mechanical and thermal stresses in components, improved component, and engine life, etc.

There are primarily four NextGen engine materials that have the potential to improve the operating conditions, safety, and performance. These four materials include:

- Ti-6Al-4V (titanium alloy):

  The benefits of this material is that it is lighter and stronger than conventional materials [36]. It can be used in engine components with low operating temperature such as fan, booster (IPC). The technology readiness level for this material's manufacturing is high, and it is implemented currently in engines. However, the use is limited because of the high costs. In future, using advanced manufacturing techniques, the production cost is expected to decrease [36], [37].
- Braided carbon composite (BCC):

  Braided composites find application to the engine casings. Specifically, in terms of application, they are best suited for casings of fan and IPC. They create lighter and more fuel-efficient engine casing, that is stronger and safer compared to the conventional materials [38], [39]. The manufacturing is matured currently and is cost-effective, and overall facilitates reduction of engine cost [38].
- Polymer matrix composite-aluminium honeycomb core (PMC/Al honeycomb):

  This is attractive for aero-engine applications because of its properties such as low weight, high strength, and low cost for manufacturing complex-shaped components. It can be used in the fan section of the engine [40].
- Ceramic matrix composites (CMCs):

  There has been a significant progress made in the development and application of CMCs consisting of silicon carbide (SiC) based matrices reinforced by small diameter continuous-length SiC-based fibres [41]. The SiC/SiC composites are currently in the early stages of implementation into hot-end components of aero gas turbine engines for civil aviation application. In comparison with the traditional materials, they offer multiple advantages because of their lighter weight and higher temperature structural capability.

There is a variety of SiC-based fibres, some of which are listed below in Table SI 8 with their densities and maximum allowable/operable temperatures.

Table SI 8. Some key properties of SiC-based fibres

SiC fibre	Density (kg/m^3)	Maximum temperature (K)
Tyranno TE	2,550 [42], [43]	1,673 [43], [44]
Hi-Nicalon	2,740 [42]	1,723 [41]
Hi-Nicalon Type-S	3,110 [42]	1,923 [41]
Tyranno SA	3,110 [42]	2,173 [41]

Table SI 9. Comparison of conventional and advanced/NextGen material densities for engine's important components

Component	Conventional		Advanced/NextGen	
	Material	Density (kg/m^3)	Material	Density (kg/m^3)
Fan casing	Ti-6Al-4V	4,429 [40], [45], [46]	BCC	1,520 [39]
Fan bypass vane	Ti-6Al-4V	4,429 [40], [45], [46]	PMC/Al honeycomb	1,533 [40]
Fan Blades and disk	Titanium-alloy (Hollow core)	2,000 [17], [47]	PMC/Al honeycomb	1,533 [40]
IPC Blades and disks	Ti-6Al-4V	4,429 [40], [45], [46]	Ti-6Al-4V	4,429 [40], [45], [46]
IPC-HPC Duct casing	Inconel 718	8,221 [48]	BCC	1,520 [39]
HPC Blades and disks	Inconel 718	8,221 [48]	Inconel 718	8,221 [48]
Combustor casing material	Inconel 718	8,221 [48]	SiC CMC (Tyranno TE)	2,550 [42]
Combustor can material	Inconel 718	8,221 [48]	SiC CMC (Tyranno SA)	3,100 [42]
HPT Blades and disks	Inconel 718	8,221 [48]	SiC CMC (Tyranno SA)	3,100 [42]
LPT Blades and disks	Inconel 718	8,221 [48]	Inconel 718	8,221 [48]

It can be seen from Table SI 8 that with SiC fibre Tyranno SA, the operable temperature can be as high as 1,900^{o}C or 2,173K. Considering the trend of turbofan engine development, the engines are becoming hotter over the time with the increase in the OPR [49]. With higher OPR, the thermal efficiency of the engine will be higher. Therefore, for the higher turbine temperatures in future engines, the use of these SiC based CMC is helpful and is required. In this work, such CMCs will be used in the hot-end components, depending on the location and need of the components. For example: Tyranno SA will be used for the combustor cans and the high-pressure turbines because these components are in direct contact with extremely hot gases. Hence, the best quality SiC fibre is selected. On the other hand, for the combustor casing (outer to the cans), CMCs are required but not the high-end SiC fibres like Tyranno SA (which can also minimise the cost). A Tyranno TE (standard) type fibre

will be used for the combustor casing. Table SI 9 provides a comparison of conventional and advanced/NextGen material densities for the engine's important components. Additionally, Table SI 10 provides a comparison of conventional and advanced/NextGen material densities for the engine's miscellaneous components. Moreover, Table SI 11 provides a comparison of mass to power ratio of conventional and advanced/NextGen gearbox. The information in Table SI 9, Table SI 10 and Table SI 11 will be used as inputs to the future engine model developed in this work and in the two validation cases (in SI §4), using GasTurb 13 software.

Table SI 10. Comparison of conventional and advanced/NextGen material densities for engine's miscellaneous components

Component	Density (kg/m^3)	
	Conventional	Advanced/NextGen engine
Shaft	4,429 [40], [45], [46]	3,204 [50]
Engine inlet casing	4,429 [17], [40], [45], [46]	1,602 [50]
Containment ring (Fan)	800 [17]	321 [50]
Inlet guide vane (IGV) of IPC	4,429 [17], [40], [45], [46]	1,602 [50]
Casing (IPC)	4,429 [17], [40], [45], [46]	1,602 [50]
IGV (HPC)	4,429 [17], [40], [45], [46]	4,429 [17], [40], [50]
Outer casing (HPC)	4,429 [17], [40], [45], [46]	4,429 [17], [40], [50]
HPC casing	4,429 [17], [40], [45], [46]	4,429 [17], [40], [50]
Outer casing (HPT)	8,221 [17], [48]	1,922 [50]
HPT casing	8,221 [17], [48]	1,922 [50]
Turbine inter-duct (HPT-LPT)	8,221 [17], [48]	3,204 [50]
LPT casing	8,220.93 [17], [48]	4,428.785 [17], [40], [50]
Exhaust casing	8,220.93 [17], [48]	4,428.785 [17], [40], [50]
Bypass casing	4,428.785 [17], [40], [45], [46]	1,601.85 [50]
Nozzle	8,220.93 [17], [48]	1,922.22 [50]

Table SI 11. Comparison of mass to power ratio of conventional and advanced/NextGen gearbox

Component	Conventional	Advanced/NextGen engine
Gearbox mass to power ratio (kg/kW)	3E-2 [17]	4.83E-3 [50]

Turbomachinery disks: Table SI 9 lists advanced material for 'disks' of compressors and turbines. These are usually the most massive components of any gas turbine engine. Disks are structurally critical, and they experience extremely high stresses and loads in the engine. Disk failure (disk burst) can be catastrophic as such failures are not containable. The turbomachinery disks will also be considered within the engine design-optimisation space in GasTurb 13. Using the advanced materials, a check is made such that the disks are not overstressed at different points in the flight envelope and that disks weigh less compared to the case of conventional materials.

SI 2.3.4 Cooling flows

It is to be noted that through all cases, advanced materials are used (as reasoned and discussed previously). Therefore, especially for hot components (combustor and HPT) the ability of advanced materials to bear high temperatures is greater compared to conventional materials. 20% cooling flows for HPT are used through all cases except Case 3 of LH_2 where the turbine cooling flow requirement is relaxed owing to the condition that the engine runs colder (reduced thrust requirement and fan size) relative to the baseline case (Jet-A), Case 1, Case 2, 100% SPK and more importantly the material's high-temperature withstanding limit. The value of 20% cooling flows for high pressure turbine is selected based on NASA's study [32] and study by Bijewitz et al. [34]. Furthermore, the engine design characteristics and thrust requirement of the study by Bijewitz et al. [34] is similar to the design requirements of this work. Therefore, the selection of 20% cooling flows in this work, for HPT, is well supported. Additionally, the study by Bijewitz et al. [34] sets design temperature limit of 1,350 K on LPT, to allow it to remain uncooled i.e. zero cooling flows. Similar condition is set in the current work (for all fuel cases), such that the LPT does not require cooling. In other words, if the temperature at the inlet of the low-pressure turbine exceeds 1,350 K, cooling flows are required. Cooling flows affect the fuel consumption since the air required for turbine cooling is extracted from the compressor. Higher the cooling flows, more is the fuel consumption.

SI 2.3.5 Combustor technology

LDI combustor uses lean combustion and is a promising low emissions combustor for aero-engines, especially for those with high OPR [51]. A continuous rise in engine OPR and turbine entry temperature (TET) because of performance requirements, results in the increase of NO_x formation. Combustors which can simultaneously meet LTO NO_x emissions regulations, achieve high efficiency, and low thrust specific fuel consumption (TSFC), are highly demanded. Other low emission technologies such as Rich-burn Quick-quench Lean-burn (RQL) have been developed and are assessed to be successful. In comparison with other low emission combustors, the LDI is shorter in length and has the potential to achieve further reduction in NO_x compared to RQL combustor. It is less likely to suffer from combustion instabilities and flashback compared to the Lean Premixed Pre-vapourised (LPP) combustor. The use of LDI combustor is advantageous because of its lean combustion, where the flame temperature is decreased by fuel combustion far (lean) from stoichiometric condition. The fuel is directly injected into the flame zone instead of being pre-vapourised and premixed with air. Therefore, the LDI combustors are less likely to suffer from auto-ignition and flashback compared to LPP combustors. The fuel injector design is thus crucial for LDI combustors to enable the required level of atomisation and homogeneous fuel-air mixing.

In this work, hydrogen is also being explored as the potential alternative to the conventional jet fuel. A review of combustors for hydrogen use is included in SI §1.3.3. One of the important technology challenges for using hydrogen in gas turbine engines is its compatibility and performance in the present combustion system, particularly the current fuel injectors. Marek et al. [13] conduct experiments with a series of novel LDI injectors for hydrogen as a potential gas turbine fuel candidate. All these injectors for hydrogen are based on LDI technology with multiple injection points and quick mixing. Flashback is one challenge

to hydrogen based premixing combustion systems because hydrogen's reaction rate is about seven times that of conventional jet fuel (Jet-A). To mitigate the risk of flashback, the mixing times were designed to be short and velocities to be high. All the LDI configurations for hydrogen combustion performed well and were stable, and these resulted in low levels of NO_x. No autoignition or flashback phenomena were encountered during the experiments. LDI combustor is found to be suitable for the use of both conventional jet fuel and hydrogen based on the above discussion. For hydrogen, C4 type of combustor configuration is preferable according to the discussion in SI §1.3.3. In this work LDI combustors (for Jet-A, 100% SPK and LH_2 [C4 type]) will be used.

SI 3. Model details

SI 3.1 Rationale for design-optimisation parameters

For the inlet standard corrected flow of engine, the extreme values are based on an educated guess. Halliwell [50] estimates the inlet standard corrected flow value of ~ 1,443 kg/s for Trent XWB engine which has a BPR of 9.3 and fan diameter of ~ 3.18 m. The design target for the engine in the present work has a BPR of 17.65 at TOC, and fan diameter of ~ 3.36 m. The inlet standard corrected flow is directly related to the fan diameter. Therefore, for a higher fan diameter and significantly higher BPR compared to the Trent XWB model by Halliwell [50], the inlet standard corrected flow has to be greater than 1,443 kg/s. The minimum, start-guess and maximum values are selected to be 1,400, 1,700 and 1,800 kg/s, respectively. Additionally, the fan diameter value of ~ 3.36 m is set as a constraint (in Table 3 in main paper) in the optimisation process of the current work as per the set design targets. The other constraint considered in this work (in Table 3), which is directly related to the inlet standard corrected flow, is the thrust. It is observed in the result section that the value of inlet standard corrected flow for the baseline (Jet-A) case is ~ 1,663 kg/s, after optimisation.

The burner exit or TET design variable has been discussed before. Since CMCs are selected for the design of hot-end components, the maximum limit is set to be 2,173 K (Tyranno SA SiC fibre) [41]. The start-guess value is 1,750 K, which is a design TET in the study by Bijewitz et al. [34]. A realistic minimum value of 1,400 K is selected as the minimum temperature limit here, though it can be set to zero as lower TETs are preferred. The optimisation constraint used here (in Table 3 in main paper), which is directly linked to the design variable of TET (T_4), is the thrust.

The minimum value of pressure ratio of any compressor must be greater than 1 for it to be called a compressor. Therefore, the minimum value of pressure ratio of fan, IPC, and HPC is set to 1.1. One of the constraints considered in this work (in Table 3) is OPR of 60, which is directly related to the pressure ratios of compressors. It is important to note that OPR is dependent on the FPR, IPC pressure ratio, and HPC pressure ratio. The design requirement states that the FPR must be 1.35, which is set as the maximum limit. The FPR is considered as a design variable primarily to try to achieve as low value as possible (<1.35) towards the set design requirements. This also results in reduced noise production, though noise evaluation is not considered in the design process explicitly throughout this work. Halliwell [50] uses a pressure ratio of 6.3 for the IPC in their turbofan engine model of an 8 stage IPC. Since, the

OPR of 60 (at TOC) as per the engine design requirement, is higher in comparison to the OPR of 50 in the study by Halliwell [50], a maximum value of 10 is used for the design variable of IPC pressure ratio. The number of stages of the IPC is previously selected to be 3 (Table SI 7), so assuming uniformly distributed compression in each stage similar to the Halliwell study [50], the start-guess value of 3 is used. The maximum value of the pressure ratio of the HPC is set to 25 considering that study by Kestner et al. [33] used a pressure ratio of 23 for the HPC. The product of the pressure losses, FPR, and IPC and HPC pressure ratio equals OPR. Since the engine OPR of 60 at the design point must be modelled and all values in the above-mentioned product except the HPC pressure ratio are known, a value of 15 suffices this product and is considered as a start-guess value for the pressure ratio of HPC.

The tip speeds of fan and HPC from the study by Halliwell [50] are used as maximum values for tip speeds for fan and HPC in this work. Tip speeds are linked to spool speeds. Since the engine currently under consideration is a geared turbofan, only the fan design speeds are expected to be different than the study by Halliwell [50] (direct-drive turbofan). Additionally, BPR and the fan diameter in the current work are greater than the study by Halliwell [50]. Therefore, the fan speeds can be expected to be very different from the study by Halliwell. The HPC speed in this work is expected to remain similar to the values in the study by Halliwell [50]. The minimum values and the start-guess values are based on the above estimation. Additionally, because the maximum values of tip speeds have been set with realistic design speeds, the spool speed has indirectly been set to realistic values. Therefore, there is an indirect design constraint considered here. This prevents high engine shaft speeds which can cause vibrations, and very high shaft speeds can lead to a phenomenon called as ‘whirling’ of shafts, which is a violent shaft vibration that could lead to shaft failure.

The study by Bijewitz et al. [34], which has almost similar design requirements, uses a maximum gear ratio of 4.5:1, and their actual design gear ratio is 4:1. The design gear ratio in the study by Kestner et al. [33] is 2.88:1, while the design gear ratio for the Pratt and Whitney’s engine PW1100G is expected to be 3:1 [52]. Therefore, the minimum, start-guess, and maximum values are selected to be 2.5, 3 and 4.5, respectively.

SI 3.2 Model inputs

Most of the model inputs are similar for baseline Jet-A fuel, 100% SPK, and all three cases of LH_2 fuel. Some of the model inputs change between baseline case and three cases of LH_2 fuel. To differentiate these changes, inputs are listed separately.

Table SI 12 lists the atmospheric data input into the engine model at off-design point of SLS. Table SI 13 lists the atmospheric data input at on-design point of TOC, and off-design point of cruise, loiter, and climb. It is to be noted that all five points, realistic values of humidity (from literature) are used, which is not used in international standard atmosphere (ISA) standards. Humidity acts as a real-world penalty on the engine thrust, and thus it is required to consider a worse case thrust in the engine design-optimisation compared to ISA. The temperature and pressure at SLS condition are standard. The altitude (35,000 ft or 10,668 m) and Mach number at cruise and TOC points are as per the design requirements discussed before (Table SI 1 – Table SI 4). Standard transport jet (civil aircraft) loiter altitude (5,000 ft or 1,500 m) and Mach number are used (from literature). Because this work uses first order modelling methods, for climb an average climb speed of 290 knots (149.19 m/s), similar to present day

efficient aircrafts like Airbus A350-900 and Boeing 787, is considered mid-way (5,334 m) of complete climb, for estimating the engine TSFC at climb [53], [54]. At the mid-way climb altitude of 5,334 m, the speed of sound is 319 m/s. Therefore, at this point 290 knots is equal to Mach number of 0.47.

Table SI 12. Atmospheric data input at off-design point of sea level static

Input parameters	SLS
Pressure	101.325 kPa [55]
Temperature	288.15 K [55]
Relative humidity	50% [55]

Table SI 13. Atmospheric data input at on-design point of top-of-climb, and off-design point of cruise, loiter and climb

Input parameters	Top of climb (TOC)	Cruise	Loiter	Climb (mid-way and average climb speed)
Altitude (m)	10,668	10,668	1,500 [56]	5,334
Relative humidity (%)	10 [57]	10 [57]	60 [57]	60 [57]
Mach number	0.8	0.84	0.6 [56]	0.47

Some of the model inputs have already been listed and discussed which include a. future engine component efficiencies (Table SI 6); b. Turbomachinery stage count (Table SI 7); c. Engine materials (Table SI 9 and Table SI 10); d. Gearbox weight to power ratio (Table SI 11); e. Engine design variables i.e., start-guess values. In this work, new engine design of the future for conventional jet fuel, 100% SPK, and LH_2 fuel (three cases), are developed using advanced material and future component efficiencies (respective inputs to the GasTurb 13 engine model), where the design requirements are set using N+2 study. In some of the validation cases only (in SI §4) conventional material and conventional component efficiencies will be input to the GasTurb 13 engine model. There are other inputs to the engine model which are listed and discussed next.

At the design point i.e., TOC, the design requirement values of BPR, bleed, and power off-take are 17.65, 0 kg/s, and 150 kW respectively, which are input to the engine model. These along with other inputs i.e., standard values from literature and GasTurb 13, are listed in Table SI 14. Recalling the discussion on OPR from SI §3.1, OPR is a product of pressure losses, FPR, IPC pressure ratio, and HPC pressure ratio. The pressure losses that count towards OPR comprise of loss in engine intake and in ducts between two consecutive compressors (fan included).

The aspect of cooling flows (input in Table SI 14) has been discussed in detail in SI §2.3.4. While most inputs remain the same for all design cases (Jet-A, 100% SPK, and three cases of LH_2), the HPC inputs viz. the HPC inlet radius ratio and HPC inlet Mach number change slightly between cases. It is to be noted that these two inputs are similar to the standard/default inputs in GasTurb 13 [17]. These are changed primarily to obtain satisfactory aerodynamic performance of the turbomachinery (discussed in §2.2 of the main paper). It can

be observed from Table SI 14 that both HPC inlet radius ratio and HPC inlet Mach number remain same for Jet-A, 100% SPK, and Case 1 of LH_2, since there is no change in engine thrust production between these cases. However, during the optimisation of Case 2 and Case 3 of LH_2, the thrust requirement and fan diameter reduces (because of lighter aircraft), which changes the shape of the HPC for maintaining the required design bypass ratio of 17.65 and thus both HPC inlet radius ratio and HPC inlet Mach number increases.

Table SI 14. Inputs for different engine components and different engine design cases (square brackets indicate reference number)

Input parameters	Value
Basic inputs for all cases (Jet-A, all three LH_2 cases, and 100% SPK)	
Intake pressure ratio	0.99 [58]
Core inlet duct pressure ratio	0.99 [17], [59]
IPC-HPC inter-duct pressure ratio	0.98 [17]
Bypass duct pressure ratio	0.992322 [17]
Turbine inter-duct reference pressure ratio	0.98 [17]
Design bypass ratio	17.65
Burner design efficiency	0.9995 [17]
Overboard bleed	0 kg/s
Power off-take	150 kW
High pressure spool mechanical efficiency	0.995 [17]
Low pressure spool mechanical efficiency	0.992 [17]
Burner pressure ratio	0.96 [50]
Turbine-exit duct pressure ratio	0.99 [17]
Fuel heating value (MJ/kg)	43.2 [1], 120 [2, 3, 4] , 44.1 [5] [11], [60]
Cooling flows	
High pressure turbine section	20% [1, 2, 3, 5] (source [32], [34]), 0% [4]
Low pressure turbine section	0% [1-5] (source [34])
Fan inputs for all cases (Jet-A, all three LH_2 cases, and 100% SPK)	
Inlet radius ratio	0.28 [17]
Inlet Mach number	0.6 [17]
HPC inputs	
Inlet radius ratio	0.423 [1, 2, 5], 0.448 [3], 0.46 [4]
Inlet Mach number	0.5 [1, 2, 5], 0.52 [3], 0.53 [4]
Inputs to be selected as per the respective case considered: [1] Baseline case (Jet-A), [2] Case 1 of LH_2, [3] Case 2 of LH_2, [4] Case 3 of LH_2, [5] 100% SPK	

Table SI 15 lists the inputs for engine nozzle section for different operating points. These inputs remain same for all design cases. Gamble et al. [61] suggest that fixed-nozzles (of gas turbine engines) have highest thrust coefficient at their design point. To account for a drop in nozzle performance at off-design point, specifically at ground conditions, an average/moderate thrust coefficient value of 0.9 is considered at SLS (off-design point) based on the study by Manneville [62], which makes this evaluation at take-off condition

(approximated to SLS for the present work). All the above-mentioned model inputs have been summarised and listed in Figure SI 7.

Table SI 15. Inputs for engine nozzle section for different operating points and different engine design cases

Input parameters	Value
SLS (Jet-A, all three LH_2 cases, and 100% SPK)	
Core and Bypass thrust coefficient	0.9 [62]
Core and bypass discharge coefficient	1 [62]
On-design (TOC), climb, cruise, and loiter (Jet-A, all three LH_2 cases, and 100% SPK)	
Core and bypass thrust coefficient	1 [63]–[65]
Design core nozzle angle	20 [50]
Design bypass nozzle angle	30 [50]

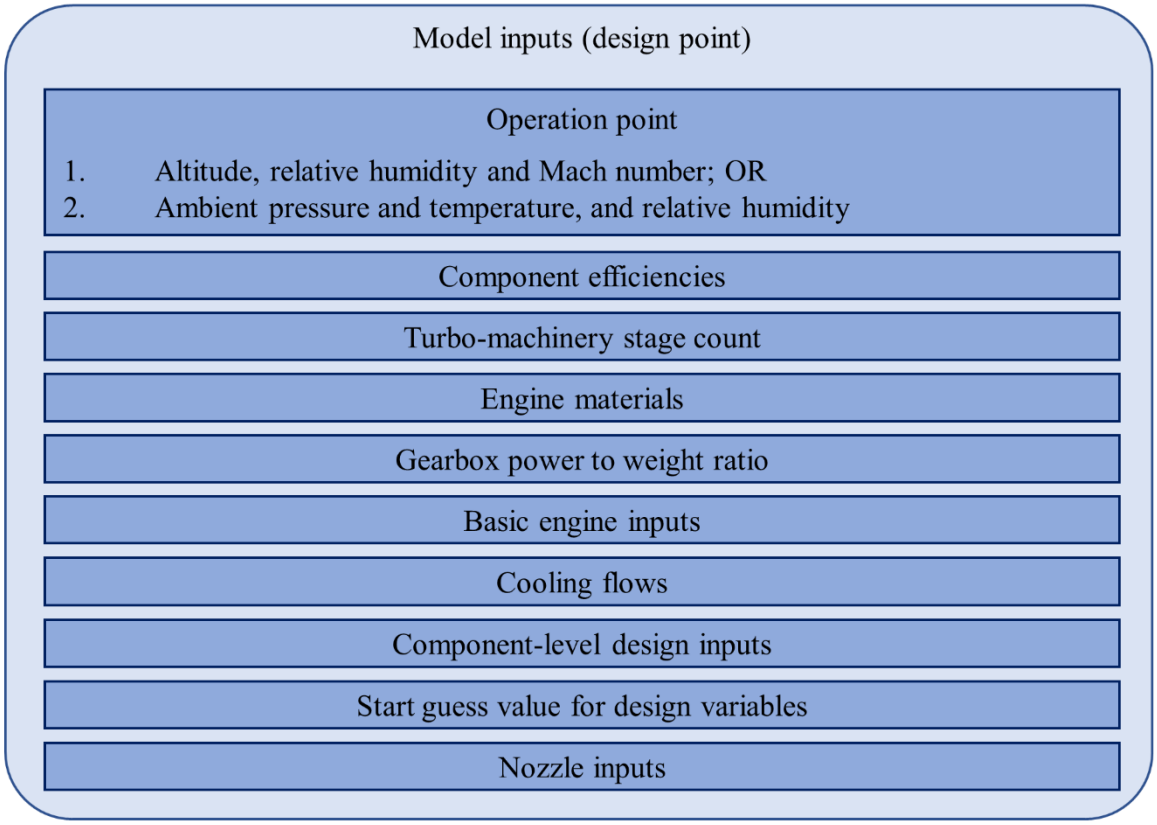

Figure SI 7. Engine model inputs

SI 4. Engine modelling validation cases

After discussing the model/methodology, it is important to try and evaluate the model using published literature. This enables to establish the model's accuracy. By conducting validation cases, a scientific confidence is built on the proposed model. In this section, there are two validation cases, and these were primarily selected because of the sufficiency of data availability (one or multiple publications) to replicate the studies. According to the book by

Kundu et al. [6] and thesis of Kirby [4], a prediction difference of ±5% is acceptable in the conceptual design phase. Therefore, for the two validation cases, this criteria of ±5% difference on engine metrics is used as a basis for establishing confidence in the model.

SI 4.1 Validation Case 1

Bijewitz et al. [34] design an UHB GTF engine for future aviation application in GasTurb 11 software. The engine data is only known for on-design point and hence this validation case is only limited to on-design point. Most of the data required for this validation case comes from study [34] and remaining information comes from another study of the same author [59] that considers same engine conditions.

Data known and methodology for case 1:

Table SI 16. On-design data of GTF engine at TOC condition of 35,000 feet (10,668 m) altitude at Mach 0.78 modelled by Bijewitz et al. [34], [59]

Parameter	Value
Basic inputs	
BPR	19.4 [34]
Fan inlet Mach number	0.7 [59]
Fan inlet Hub/Tip Ratio	0.29 [59]
Intake pressure ratio	0.997 [59]
Core intake pressure ratio	0.99 [59]
Bleed and power off-take	None [34]
Number of fans, IPC, HPC, HPT, LPT stages	1, 3, 9, 2, 4 [34]
Gear ratio	4:1 [34]
TET or T_4	1,750 K [34]
Cooling flows	
Cooling flows	20% for HPT; 0% for LPT [34]
Constraints	
Thrust	56 kN [34]
OPR	60 [34]
Fan diameter	3.35 m
Performance parameters	
TSFC	12.67 g/s-kN [34]
Core efficiency	0.6 [34]
Propulsive efficiency	0.85 [34]
Thrust/engine mass flow	83 [34]
OR	OR
Engine mass flow	674.6 kg/s

The data known for the validation case 1 is summarised in Table SI 16. The process of design-optimisation remains the same as discussed in the methodology section in the main paper. Table SI 16 also categorizes the data from the studies of Bijewitz et al. [34], [59] into

inputs, cooling flows, constraints, and performance parameters. The design requirement here is to design a UHB GTF engine with a BPR of 19.4, OPR of 60, fan diameter 3.35 m, and to produce thrust of 56 kN at TOC point of 35,000 feet (10,668 m) altitude with Mach 0.78 [34].

The fuel used here is Jet-A, and cooling flows are 20% for HPT with uncooled LPT [34]. The number of fan, IPC, HPC, HPT, and LPT stages are 1, 3, 9, 2, and 4, respectively [34]. The fan inlet Mach number and hub/tip ratio are 0.7 and 0.29, respectively [59]. There is no power off-take and bleed [34]. The pressure ratios at engine inlet and core inlet are 0.997 and 0.99 respectively [59]. Bijewitz et al. [34] use conventional material in the engine except the fan, where they use PMC. The properties of conventional material (including gearbox technology) and PMC are known from Table SI 9 – Table SI 11. The above information/inputs need to be updated in the model described in the methodology section in the main paper.

The component efficiency for each turbomachine is unknown through the studies of Bijewitz et al. [34], [59], and therefore all component efficiencies will be treated as design variables in the optimisation process, unlike the methodology section in the main paper. For all these design variables, all minimum values are set to 0.85, the start-guess values are set to the values in Table SI 5 (present efficiencies) and the maximum values are set to values in Table SI 6 (future efficiencies at TOC point). Also, compared to the proposed model, the design TET and gear ratio are known to be 1,750 K and 4:1, respectively. Hence, these two parameters, which are design variables in the methodology section in the main paper, will be removed as design variables as these values are fixed as per the known data/design requirement.

The design constraints (parameters) remain the same, except the change in their values. Thus, 56 kN of thrust is to be produced with an engine which has OPR of 60 and fan diameter of 3.35 m. Overall, the model described in the methodology section of the main paper, remains unchanged (including all model inputs) except the changes/updates mentioned above as they are pertinent to replicate the studies of Bijewitz et al. [34], [59] listed in Table SI 16. The methodology for this validation case is now completed, and the results are discussed below, along with a comparison of engine performance with the published values.

Validation case 1 results and discussion:

Table SI 17 shows the comparison of on-design engine performance between the current model and study by Bijewitz et al. [34]. It can be observed from Table SI 17 that the proposed model in the main paper is able to replicate the study by Bijewitz et al. [34] with high accuracy (+0.035% difference in the TSFC values between both studies relative to Bijewitz et al. [34]) and meet all design requirements (italicised). The LPT inlet temperature in both cases is lower than 1,350 K which was a requirement for having uncooled LPT.

In terms of engine weight, the study by Bijewitz et al. [34] does not provide engine weight directly, instead it gives the total propulsion system weight (of 7,648 kg). Additionally, the breakdown of the total propulsion system weight into component weights, is not provided by Bijewitz et al. [34]. Moreover, it is not clear whether the total propulsion system weight (of 7,648 kg) is inclusive of engine mount weight. Therefore, there are two different engine weights estimated in Table SI 18: 1. Inclusive of weights of the bare engine, nacelle and inlet, and mount; 2. Inclusive of weights of the bare engine, nacelle, and inlet only. The bare engine weight is calculated using GasTurb 13 as discussed previously. The nacelle and inlet weight, and mount weight, both come from Table SI 2 i.e. from the NASA N+2 study by Nickol et al.

[30]. It is to be noted that the engine weight calculation (with disk optimisation) is not as rigorous as discussed in the methodology section in the main paper, because the off-design points are not considered by Bijewitz et al. [34]. Therefore, disk weight optimisation, and resultantly the bare engine weight estimation, is just limited to the on-design point.

Table SI 17. Comparison of on-design engine performance between the current model and study by Bijewitz et al. [34]

TOC		Bijewitz et al. [34]	Present model
		GasTurb 11	GasTurb 13
Mach, Altitude	- , m	0.78 at 10,668 m	0.78 at 10,668 m
Net Thrust	*kN*	*56*	*56.6*
Thrust difference with respect to Bijewitz et al. [34]	%	-	+ 1.071
OPR		*60*	*60*
BPR		*19.4*	*19.4*
Fan diameter	*m*	*3.35*	*3.35*
Number of Fan, IPC, HPC, HPT, LPT stages		1, 3, 9, 2, 4	1, 3, 9, 2, 4
Engine mass flow	kg/s	674.6	674.4
TSFC	g/kN-s	12.67	12.6744
TSFC difference with respect to Bijewitz et al. [34]	%	-	+ 0.035
Fuel consumption (FC)	kg/s	0.71	0.71
Gear ratio		4	4
Cooling flow	%	20	20
TET or T_4	K	1750	1750
Power off-take and bleed		None	None
Core efficiency		0.6	0.6
Propulsive efficiency		0.85	0.85
LPT inlet temperature	K	< 1,350	1,207.08

There are two different cases considered in Table SI 18. The first case is the known case, where PMC material is used for the fan section and for other components conventional materials are used. Ideally, 'total propulsion system weight' should be the first type of weight calculation i.e. inclusive of weights of the bare engine, nacelle, and inlet and mount, and its estimation by the proposed model is highly accurate (well within the ±5% difference criteria) compared to the study by Bijewitz et al. [34]. Recalling the value of 1,750 K for the design-point TET i.e. at TOC point from the study by Bijewitz et al. [34], it would mean that at SLS conditions the TET would be of the order of 2,000K which is very high for conventional materials (used by Bijewitz et al. [34]) to withstand a successful engine operation. Bijewitz et al. [34] mention that their maximum limit for TET is 2,050 K. Clearly, it is necessary to use CMCs as these are the only materials that can withstand such high temperatures. Thus, a second case is considered and is listed in Table SI 18, where PMC is used in fan, CMCs are used in hot sections, and conventional materials in other components. In the second case considered

here, only the present model adheres to the changes (CMC use). The total engine weight of Bijewitz et al. [34], remains unchanged compared to the first case. The second case highlights the need to use CMCs in hot components, not only from realistic engine operability perspective but also its potential of engine weight reduction. Since this (second case) is a hypothetical or proposed case, there is no basis for a direct comparison of weights and thereby no validation process is conducted.

Table SI 18. Comparison of total engine weights between the current model and study by Bijewitz et al. [34]

First case: PMC for fan section and conventional materials in other components				
		Bijewitz et al. [34]	Present model	% Difference
Bare engine weight	kg	-	6,738	-
Total engine weight [1]	kg	7,648	7,651	+ 0.039
Total engine weight [2]	kg	7,648	7,514	- 1.752
Second case: PMC for fan section, CMC for hot sections and conventional materials in other components				
Engine weight	kg	-	6,629	-
Total engine weight [1]	kg	7,648	7,543	-
Total engine weight [2]	kg	7,648	7,406	-

[1] Inclusive of weights of the bare engine, nacelle and inlet and mount.
[2] Inclusive of weights of the bare engine, and nacelle and inlet only

The thrust and TSFC values are estimated with +1.071% and +0.035% difference, respectively. In terms of weights, the first type and the second type of total weight calculation have +0.039% and – 1.752% difference, respectively. These predictions fall well within the set criteria of prediction difference of ±5% from literature for a successful conceptual design. Overall, it is observed that the proposed model estimated the engine performance and weight, with a high accuracy in comparison with the study by Bijewitz et al. [34]. This concludes the first validation case. A second validation case is considered next, as a sanity check towards establishing confidence on the proposed model.

SI 4.2 Validation Case 2

Nickol et al. [30] design a UHB GTF engine powered by Jet-A for NASA N+2 timeframe of aviation use, using the NPSS software. The engine data is only known for on-design point and one off-design point (of SLS). However, the component efficiencies are not known for both these points. Thus, the current validation case is limited only to on-design point with three possible cases of component efficiencies. It is to be noted that this is the same study (Nickol et al. [30]) which is used as a reference study to establish the aircraft and engine design targets towards the objective of the current work. The engine design requirement (on-design/TOC point only) of this validation case is exactly similar to the design requirements of the proposed model described in the methodology section of the main paper, because these are based on same study by Nickol et al. [30].

Data known and methodology for case 2:

For this validation case, all known data is already included in the methodology section of the main paper. The model setup remains unchanged except for few parameters discussed below. As discussed in detail in the methodology section of the main paper, the stage counts of turbo-machineries are not known from the study by Nickol et al. [30]. Therefore, the selection of turbomachinery stage counts is based on three different studies, and this selection process is discussed previously in SI §2.3.2. The number of Fan, IPC, HPC, HPT, and LPT stages are 1, 3, 9, 2, and 3, respectively, as listed in Table SI 7 earlier, and these are assumed to remain unchanged for this validation case. The model inputs remain the exact same except component efficiencies and materials. It is to be noted that in terms of materials, CMC is the only material known to be used in the study by Nickol et al. [30] in their engine design for hot sections. Therefore, it is assumed that conventional materials are used for all engine components except the combustor and HPT, where CMC is used. However, it is very likely that PMC 'might' be used in the engine fan section by Nickol et al. [30], though not considered in this validation case. Additionally, cooling flows, gear ratio and pressure ratios of compressors are unknown. 20% cooling flows are assumed, as mentioned also in SI §2.3.4. Gear ratio, and pressure ratios of IPC and HPC, are treated as design variables in optimisation, which is exactly similar to the proposed model in in the methodology section of the main paper.

As mentioned above, the component efficiencies are not known from the study by Nickol et al. [30]. Therefore, at on-design point three cases of component efficiencies are used towards this validation case. In the first and second case, future component efficiencies and conventional component efficiencies are used, respectively. For both cases, the optimisation scheme also remains unchanged. In the third case, all component efficiencies will be treated as design variables in the optimisation process (similar to validation case 1), unlike the proposed model in the methodology section of the main paper. For all these design variables, all minimum values are set to 0.85, the start-guess values are set to the values in Table SI 5 (present efficiencies), and the maximum values are set to values in Table SI 6 (future efficiencies at TOC point). Additionally, in this third case, a constraint-target of TSFC (13.1543 g/kN-sec) is added to the model that enables the exact replication of NASA N+2 study by Nickol et al. [30]. By doing this, the exact component efficiencies can be found by reverse-engineering for a fixed/known target TSFC.

Overall, the model described in the methodology section of the main paper, remains unchanged (including all model inputs) except the changes/updates mentioned above. The methodology for this validation case is now completed, and the results are discussed below, along with a comparison of engine performance with the published values.

Validation case 2 results and discussion:

Table SI 19 provides the comparison of on-design/TOC engine performance and weights between the study by Nickol et al. [30] and three cases of the present model. The three cases are:

- 1st case: Future component efficiencies are used,
- 2nd case: Conventional component efficiencies are used,

- 3rd case: All component efficiencies are treated as design variables (future component efficiencies treated as the maximum limit for these design variables) in optimisation, with TSFC set as a design constraint-target (of 13.1543 g/kN-sec).

Table SI 20 provides the comparison of component efficiencies between the three cases of the present model. It is to be noted that the component efficiencies listed for the 3rd case are the output of the optimisation process. It can be observed from Table SI 20 that the proposed model (all three cases) exactly meets all design requirements (italicised). The LPT inlet temperature in all three cases of the present model are below 1,350 K, which was a requirement for having uncooled LPT.

Table SI 19. Comparison of on-design/TOC (Mach 0.8 at 10,668 m) engine performance and weights between the study by Nickol et al. [30] and three cases of the present model

Parameters	Units	Nickol et al. [30]	1st case	2nd case	3rd case
Net thrust	*kN*	*55.603*	*55.603*	*55.603*	*55.603*
OPR		*60*	*60*	*60*	*60*
BPR		*17.65*	*17.65*	*17.65*	*17.65*
FPR		*1.35*	*1.35*	*1.35*	*1.35*
Fan diameter	*m*	*3.36296*	*3.36296*	*3.36296*	*3.36296*
Engine mass flow	kg/s	-	638.06	638.06	638.06
TSFC	g/kN-s	13.1543	12.3997	13.2694	13.1543
FC	kg/s	0.731	0.689	0.7378	0.7314
TSFC/FC difference with respect to Nickol et al. [30]	%	-	- 5.737	+ 0.875	0
Bare engine weight	kg	6,789	6,992	7,170	7,150
Bare engine weight difference with respect to Nickol et al. [30]	%	-	+ 2.99	+ 5.612	+ 5.317
Gear ratio		-	3.5	3.5	3.5
Cooling flow	%	-	20	20	20
Ratio of temperatures at turbine entry and fan inlet (T_4/T_2)		-	6.844	7.06	7.05
Power off-take	kW	150	150	150	150
LPT inlet temperature	K	-	1,139	1,186	1,180

It can be observed from Table SI 19 that compared to the study by Nickol et al. [30], the TSFC and/or FC for: the 1st case is 5.737% lower, the 2nd case is slightly higher (i.e. +0.875% difference), and 3rd case is equal (as TSFC was a constraint-target in the 3rd case) [0% error]. This is primarily because of the component efficiencies. The 1st case uses future component efficiencies, whereas 2nd case uses present day efficiencies, which results in the above-mentioned difference in TSFCs and/or the FC values. It can be observed from Table SI 20 that there is less difference between the component efficiencies of 2nd case and 3rd case. It means that the present day component efficiencies are similar to the optimum component efficiencies that enables the 3rd case to meet the exact TSFC and/or FC value of the study by Nickol et al. [30], and the TSFC and/or FC of 2nd case is similar/slightly higher (i.e. +0.875%

difference) compared to the said study. Additionally, with the assumptions made here, it appears that the study by Nickol et al. [30] might have used present day component efficiencies.

It can be observed from Table SI 19 that the engine weights of the 1st case, 2nd case and 3rd case, compared to the engine weight from the study by Nickol et al. [30], are greater by approximately 200 kg (+2.99% difference), 380 kg (+5.61% difference), and 360 kg (+5.32% difference), respectively. These differences in engine weights are attributable to the unknowns from the study by Nickol et al. [30] such as:

- Engine materials,
- Turbo-machinery stage count,
- Gear ratio,
- Pressure ratios of IPC and HPC,
- Cooling flows, and
- Component efficiencies

Table SI 20. Comparison of component efficiencies between the three cases of the present model

Components		Component efficiencies		
		1st case [32]	2nd case [17]	3rd case
Fan	Inner	0.928	0.910	0.902
	outer		0.904	0.912
IPC		0.925	0.920	0.920
HPC		0.912	0.910	0.908
HPT		0.944	0.890	0.896
LPT		0.956	0.922	0.925

The engine material selection has direct impact on the engine weight. CMC is the only material known to be used in the hot section of the engine modelled by Nickol et al. [30] and therefore assumption was made to use conventional materials in all components except HPT and combustor. As mentioned before, is very likely that PMC 'might' be used in the engine fan section by Nickol et al. [30] in their study. Additionally, parameters that are directly linked to each other such as gear ratio, IPC and HPC pressure ratio, and turbomachinery stage count and efficiencies, all have a considerable impact on the engine weight. Moreover, cooling flows can significantly affect both the TSFC (directly) and weight (indirectly). Lastly, it is to be noted that the engine weight calculation (with disk optimisation) conducted here is not as rigorous as discussed in the methodology section of the main paper, because the off-design points are not considered here (as reasoned before while defining the scope of this validation case). Therefore, disk weight optimisation, and resultantly the bare engine weight estimation, is just limited to the on-design point.

In the first case, where the model uses future component efficiencies, the model predicts TSFC or FC and bare engine weight with -5.74% and +2.99% difference, respectively. For the second case, where the model uses present component efficiencies, the model predicts TSFC or FC, and bare engine weight with +0.875% and +5.612% difference, respectively. Lastly for the third case, where the model component efficiencies are set as design variables, the model predicts TSFC/FC and bare engine weight with 0% and +5.317% difference,

respectively. As mentioned above, second and third case appear to be realistic and closer to study by Nickol et al. [30]. Therefore, for these two cases, it is observed that the proposed model estimates the engine TSFC and FC with high accuracy (<0.88% difference) as compared to the study by Nickol et al. [30]. These predictions are well within the set criteria of prediction difference of ±5% from literature for a successful conceptual design. In terms of engine weights, there are is a lot of unknown information in the study of Nickol et al. [30], which is underscored and discussed above in detail. For the second and third case, there is a difference of +5.612% and +5.317% in bare engine weight, respectively. Despite these mentioned unknowns, the model predicts engine weights with reasonable accuracy. These predictions are similar in magnitude to the set criteria of prediction difference of ±5% from literature for a successful conceptual design. This concludes the second validation case.

SI 4.3 Conclusion of the validation cases

The proposed model can successfully replicate the engine performance in both validation cases, considered in this section. It is observed that the success of the validation process is also dependent on the pool of the known information from the study to be replicated. In the first validation case, the proposed model predicted both engine performance and its weight with high accuracy, where both performance metrics and engine weight predictions fall well within the set criteria of prediction difference of ±5%. In the second validation case, the proposed model predicted the engine performance with high accuracy, and the accuracy of engine weight prediction was reasonable despite not knowing the critical engine design parameters from the study to be replicated i.e. study by Nickol et al. [30]. In the second case, TSFC and FC predictions are well within the set criteria of prediction difference of ±5% from literature for a successful conceptual design; and the bare engine weight prediction by the model, despite a plethora of identified unknowns, provided predictions that are similar in magnitude to the set criteria of prediction difference for a successful conceptual design. This can therefore be considered a satisfactory validation process. Overall, a strong confidence has now been developed on the proposed model, through this scientific procedure.

SI 5. Results and discussion

SI 5.1 Baseline Jet-A engine 6-21

Table SI 21 and Table SI 22 lists the on-design (TOC) and off-design (SLS) engine performance of the present Jet-A engine design, respectively. Also, there are other studies based on future engine technologies listed in both tables (depending on data availability) which have unique engine configurations and are relevant to this work, though cannot be used for direct comparison.

Table SI 21. Engine performance of the present model and other studies [30], [32]–[34] **using Jet-A fuel at TOC condition**

Parameters	Units	Operating point unknown	TOC			
		Kestner et al. [33]	Greitzer et al. [32]	Bijewitz et al. [34]	Nickol et al. [30]	Present design
Mach, altitude	- , m	Unknown	~0.8 at 10,668 m	0.78 at 10,668 m	0.8 at 10,668 m	0.8 at 10,668 m
Engine mass flow	kg/s	-	512	674.6	-	638.1
Net thrust	kN	-	44	56	55.603	55.603
TSFC	g/kN-s	14.333	14.47	12.67	13.1543	12.3997
Fuel consumption	kg/s	-	0.637	0.71	0.731	0.689
OPR	-	46	55.2	60	60	60
BPR	-	20.29	19.44	19.4	17.65	17.65
FPR	-	1.353	1.46	-	1.35	1.35
Fan diameter	m	3.079	-	3.35	3.36296	3.36296
Bare engine weight	kg	4,515	-	7,648*	6,789	4,411
Gear ratio	-	2.88	-	4	-	3.5
Cooling flow	%	-	20	20	-	20
T_4/T_2	-	-	7	7.12	-	6.84
Power off-take	kW	-	-	0	150	150
LPT inlet temperature	K	-	-	< 1,350	-	1,139

* is total propulsion system weight and not bare engine weight, T_2 is the fan inlet temperature

Table SI 22. Engine performance of the present model and other studies [30], [32] **using Jet-A fuel at SLS condition**

SLS parameters	Units	Greitzer et al. [32]	Nickol et al. [30]	Present design
Engine mass flow	kg/s	1,119	-	1,527
Net thrust	kN	261.4	299.9	303.9
TSFC	g/kN-s	6.12	5.62	5.12
Fuel consumption	kg/s	1.6	1.69	1.56
OPR	-	52.8	47.1	47.1
BPR	-	18.86	20	20
FPR	-	1.43	1.25	1.25
Cooling flow	%	20	-	20
T_4/T_2	-	6.60	-	6.16
Power off-take	kW	-	150	150
LPT inlet temperature	K	-	-	1,213

A study by Kestner et al. [33] on N+2 aviation technology is listed in Table SI 21. However, the point of engine operation is not known. It is listed as a reference point for engine weight, though the materials used in the said study are not disclosed by the authors. A study by Bijewitz et al. [34] is also listed in Table SI 21, and it is used in the first validation case (in SI §4.1). Another study by Greitzer et al. [32] is also listed both in Table SI 21 and Table SI 22. Both studies (Bijewitz et al. [34] and Greitzer et al. [32]) different BPR and OPR combination but are relevant as they model futuristic technology engine. Moreover, the propulsion system in the Greitzer et al. study [32] has four fans driven by two engine cores, compared to a single fan driven by one engine core via gearbox in the current work. Therefore, these studies cannot be used for direct comparison. In the present work, the future component efficiencies are used and these come from the study by Greitzer et al. [32] and it also provides T_4/T_2 value, which gives some reference point for temperature values of future (efficient) engine technologies. Only the study by Nickol et al. [30] (also used in the second validation case in SI §4.2) is directly relevant to the Jet-A engine design of the present work (in Table SI 21 and Table SI 22) since this study sets the design requirements (listed in Table 3).

It can be observed from Table SI 21 and Table SI 22 that the Jet-A engine design meets all design requirements at the TOC and SLS condition, which are set in Table 3. The effect of high values of future component efficiencies is reflected in the lower TSFC and/or fuel consumption values of the present Jet-A engine design in comparison with the study by Nickol et al. [30]. In line with this effect, the turbine inlet temperature (TET or T_4) of the present work is also lower than the studies by Bijewitz et al. [34] and Greitzer et al. [32]. As observed from Table SI 21, the use of advanced materials throughout the engine has resulted in significant reduction (~35%) in engine weight compared to the study by Nickol et al. [30]. The present Jet-A engine weight estimated in this work is similar to the engine weight of the study by Kestner et al. [33]. The engine performance at other off-design points for Jet-A engine i.e., cruise, and loiter and climb, is included in SI §5.1 in Tables SI 23 and SI 24, respectively. Additionally, the performance of engine powered by 100% SPK is similar to Jet-A engine, as expected, due to similar fuel properties, at on-design point (TOC) and all four off-design points (SLS, climb, cruise, and loiter). These are included in SI §5.2 in Tables SI 25 – SI 29.

Table SI 23 shows the off-design engine performance (cruise condition) of the present Jet-A engine design and of other studies. It can be observed from Table SI 23 that the impact of high values of future component efficiencies can be seen at cruise conditions also. The use of very high efficiency turbomachinery components have resulted in lower engine TSFC and/or fuel consumption values in the present Jet-A engine design compared to the study by Nickol et al. [30]. On similar lines, the TET of the present design is also lower compared to the study by Greitzer et al. [32]. An LTA aircraft spends 90+% of the flight time in cruise. The lower TSFC value is expected to result into significant savings in fuel consumption over one flight mission. For cruise condition, the lift force equals aircraft weight, and thrust is equal to drag force. In cruise, thrust to weight ratio (T/W) is equal to the reciprocal of the lift to drag ratio (L/D) ratio of the aircraft. The calculation of the L/D ratio is done separately through aerodynamic equations, and the aircraft weight is estimated in the aircraft weight sizing process. This calculates the unknown value of required thrust. The process for thrust requirement calculation is discussed in detail, in [66]. In Table SI 23, the engine produces 51.61 kN of thrust where the minimum required thrust is calculated to be 42.25 kN.

Table SI 23. Engine performance of the present model and other studies [30], [32] **using Jet-A fuel at cruise condition**

Cruise parameters	Units	Greitzer et al. [32]	Nickol et al. [30]	Present design
Mach, altitude	- , m	0.83 at ~10,668 m	0.84 at 10,668 m	0.84 at 10,668 m
Engine mass flow	kg/s	484	-	649.7
Net thrust	kN	36.9	-	51.6
TSFC	g/kN-s	14	13.455	12.667
Fuel consumption	kg/s	0.517	-	0.654
Cooling flow	%	20	-	20
T_4/T_2	-	6.60	-	6.57
Power off-take	kW	-	150	150
LPT inlet temperature	K	-	-	1,107

Table SI 24. Engine performance of the present engine model using Jet-A fuel at loiter and climb conditions

Parameters	Units	Present Jet-A engine design	
		Loiter	Climb (mid-way and average climb speed)
Mach, altitude	- , m	0.6 at 1,500 m	0.47 at 5,334 m
Engine mass flow	kg/s	1,488.32	904.96
Net thrust	kN	114.67	94.94
TSFC	g/kN-s	12.175	9.798
Fuel consumption	kg/s	1.396	0.931
Cooling flow	%	20	20
T_4/T_2	-	5.741	6.315
Power off-take	kW	150	150
LPT inlet temperature	K	1,167	1,129

Table SI 24 shows the off-design engine performance of the present Jet-A engine design at points of loiter and climb. There are no studies that can be used either for comparison or providing some reference values. It is to be noted that the LPT inlet temperatures at all points (on-design and off-design) in the present Jet-A engine design are lower than 1,350 K which was required for having uncooled LPT. This design choice was successful primarily because of the use of future component efficiencies. Figure SI 8 shows the cross-sectional view of the Jet-A powered GTF engine designed from the proposed/present model. This figure also shows the diameter of the fan (a design requirement) and length of the engine. The 'I-section' of the turbomachinery disk, a design choice, can be noticed in Figure SI 8.

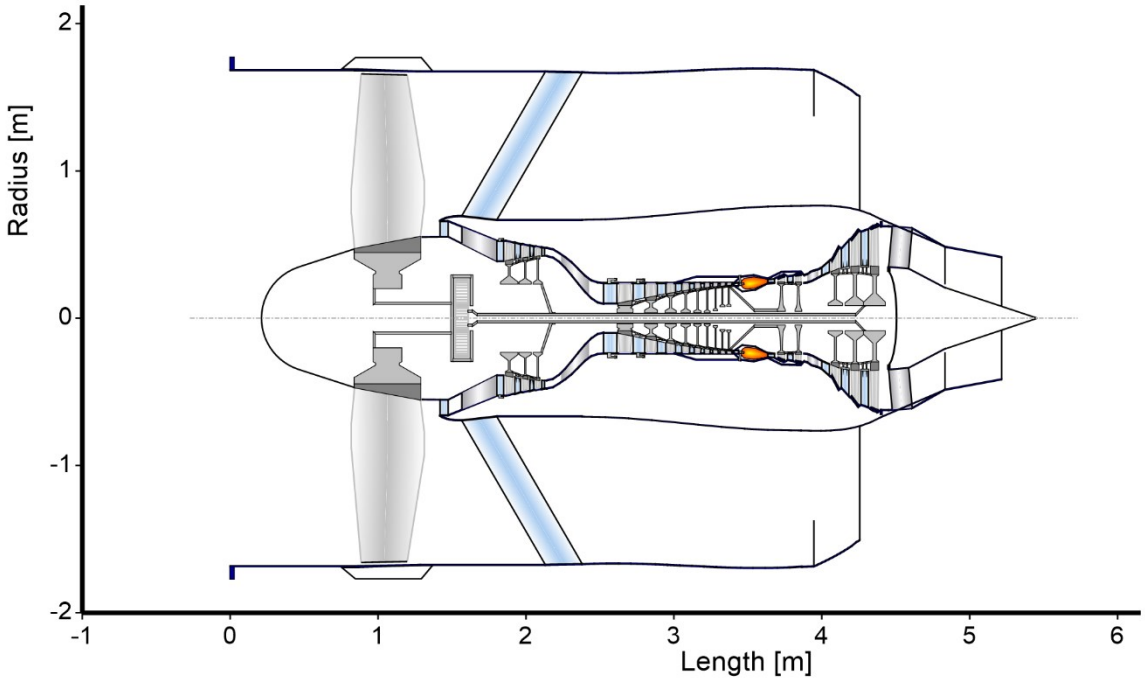

Figure SI 8. Cross-sectional view of the Jet-A powered GTF engine designed using the proposed model

Overall, the use of future component efficiencies in the present Jet-A engine design, has improved the fuel efficiency of the engine at all operational points considered in this work, which is as per expectation. A significant reduction (~35%) in engine weight (compared to the study by Nickol et al. [30]) is observed primarily because of two reasons: use of advanced materials, and the turbo-machinery stage count selection process (SI §2.3) along with satisfactory aerodynamic performance of turbomachinery (§2.2 of the main paper). The TSFC values for the present Jet-A engine design at all operational points considered in this work, are inputs to the aircraft weight sizing process discussed in [66]. This enables the estimation of fuel burn of the aircraft over one mission. The above discussion concludes the Jet-A UHB GTF engine on-design and off-design analysis.

SI 5.2 100% SPK engine

In this section 100% SPK fuel is being investigated. The lower heating value (LHV) of 100% SPK fuel is known to be 44.1 MJ/kg, as compared to LHV of Jet-A of 43.2 MJ/kg. As a result, slightly lower mass of SPK fuel must be carried at the beginning of the flight mission. Therefore, the 100% SPK aircraft weight at different points in flight mission is lower than the Jet-A case resulting in slight efficiency improvement (discussed in [66]), which is also observed in our previous study [31]. The process for thrust requirement calculations is discussed in detail, in [66]. Tables SI 25, SI 26, SI 27, SI 28, and SI 29 list the comparison of engine performance using Jet-A and 100% SPK, at TOC (on-design point), SLS, cruise, climb, and loiter points, respectively. It can be observed from Table SI 25 - Table SI 27 that the thrust requirement for 100% SPK at TOC, SLS and cruise is insignificantly lower than Jet-A case. Therefore, the thrust production for the 100% SPK is kept similar to Jet-A case.

Table SI 25. Comparison of engine performance at TOC condition using 100% SPK and Jet-A, using the proposed model

TOC parameters	Units	Jet-A	100% SPK
Mach, altitude	- , m	0.8 at 10,668 m	
Engine mass flow	kg/s	638.1	
Thrust required	kN	55.603	55.24
Thrust produced	kN	55.603	
TSFC	g/kN-s	12.40	12.15
Fuel consumption	kg/s	0.689	0.676
Fuel-air ratio (FAR)	-	0.025191	0.024684
Equivalence ratio (Φ)	-	0.37	0.36
OPR	-	60	
BPR	-	17.65	
FPR	-	1.35	
IPC pressure ratio	-	3.296	
HPC pressure ratio	-	13.9	
Cooling flow	%	20	
Combustor length	m	0.1981	
Combustor gas velocity	m/s	235.68	235.80
Residence time	ms	0.841	
P_3	kPa	2159.43	
T_3	K	859	
T_4	K	1,690	1,691
T_4/T_2	-	6.844	6.850
Bare engine weight	kg	4,411	4,410
Gear ratio	-	3.5	
Fan diameter	m	3.36296	
LPT inlet temperature	K	1,139	1,140
Power off-take	kW	150	

P_3: Total pressure at combustor inlet, T_3: Total temperature at combustor inlet

It can be observed from Table SI 25 - Table SI 27 that the engine designs successfully meet the design requirements/targets as set in Table 3 and Table SI 4. In Table SI 25 - Table SI 27, the engine designs meet the required thrust values for 100% SPK, at said mission points considered in these tables. These thrust requirements are calculated through the aircraft weight sizing process (details in [66]).

The slight increase in LHV (as detailed above) of 100% SPK as compared to Jet-A improves its TSFC. This can be observed from Table SI 25 - Table SI 29. The slightly higher LHV of 100% SPK as compared to Jet-A, causes an insignificant rise in their respective T_4 which can be observed from Table SI 25 - Table SI 29. Additionally, it is to be noted that the LPT inlet temperatures at all points (on-design and off-design) in engine designs listed in Table SI 25 - Table SI 29, are lower than 1,350 K which was required for having uncooled LPT. This design choice was successful primarily because of the use of future component efficiencies.

The engine diameter does not change between Jet-A case and 100% SPK (design constraint as per Table 3 and Table SI 4). The bare engine weight is similar for Jet-A case and 100% SPK as listed in Table SI 25.

Table SI 26. Comparison of engine performance at SLS condition using 100% SPK and Jet-A, using the proposed model

SLS parameters	Units	Jet-A	100% SPK
Mach, altitude	- , m	0 at 0 m	
Engine mass flow	kg/s	1,526.97	1,526.89
Thrust required	kN	299.9	301.8
Thrust produced	kN	303.9	303.9
TSFC	g/kN-s	5.124	5.022
Fuel consumption	kg/s	1.557	1.526
FAR	-	0.026912	0.026371
Φ	-	0.39	0.38
OPR	-	47.1	
BPR	-	20	
FPR	-	1.25	
IPC pressure ratio	-	3.028	3.028
HPC pressure ratio	-	12.769	12.768
Cooling flow	%	20	
Combustor length	m	0.1981	
Combustor gas velocity	m/s	241.78	241.91
Residence time	ms	0.82	0.82
P_3	kPa	4,724.82	4,724.26
T_3	K	914	914
T_4	K	1,776	1,777
T_4/T_2	-	6.163	6.168
LPT inlet temperature	K	1,213	1,213
Power off-take	kW	150	

Table SI 27. Comparison of engine performance at cruise condition using 100% SPK and Jet-A, using the proposed model

Cruise parameters	Units	Jet-A	100% SPK
Mach, altitude	- , m	0.84 at 10,668 m	
Engine mass flow	kg/s	649.65	649.67
Thrust required	kN	42.25	42.16
Thrust produced	kN	51.61	
TSFC	g/kN-s	12.667	12.411
Fuel consumption	kg/s	0.654	0.641
FAR	-	0.024099	0.023613
Φ	-	0.35	0.34
Combustor length	m	0.1981	
Combustor gas velocity	m/s	231.99	232.11
Residence time	ms	0.854	
P_3	kPa	2,108.3	2,108.4
T_3	K	838	838.
T_4	K	1640	1641
T_4/T_2	-	6.567	6.572
Cooling flow	%	20	
LPT inlet temperature	K	1,107	1,108
Power off-take	kW	150	

Table SI 28. Comparison of engine performance at climb condition using 100% SPK and Jet-A, using the proposed model

Climb parameters	Units	Jet-A	100% SPK
Mach, altitude	- , m	0.47 at 5,334 m	
Engine mass flow	kg/s	904.96	904.99
Thrust produced	kN	94.94	94.95
TSFC	g/kN-s	9.798	9.599
Fuel consumption	kg/s	0.930	0.912
FAR	-	0.024524	0.02403
Φ	-	0.36	0.35
Combustor length	m	0.1981	
Combustor gas velocity	m/s	234.3	234.4
Residence time	ms	0.846	
P_3	kPa	2,978.5	2,978.8
T_3	K	861	861
T_4	K	1672	1673
T_4/T_2	-	6.315	6.321
Cooling flow	%	20	
LPT inlet temperature	K	1,129	1,129
Power off-take	kW	150	

Table SI 29. Comparison of engine performance at loiter condition using 100% SPK and Jet-A, using the proposed model

Loiter parameters	Units	Jet-A	100% SPK
Mach, altitude	- , m	0.6 at 1500 m	
Engine mass flow	kg/s	1,488.32	1,488.41
Thrust produced	kN	114.67	114.70
TSFC	g/kN-s	12.175	11.929
Fuel consumption	kg/s	1.396	1.368
FAR	-	0.024892	0.024394
Φ	-	0.36	0.36
Combustor length	m	0.1981	
Combustor gas velocity	m/s	237	237.6
Residence time	ms	0.835	0.834
P_3	kPa	4,486	4,487
T_3	K	905	905
T_4	K	1,713	1,715
T_4/T_2	-	5.741	5.746
Cooling flow	%	20	
LPT inlet temperature	K	1,167	1,167
Power off-take	kW	150	

SI 5.3 LH_2 engine

Tables SI 30, SI 32, SI 33, SI 34, and SI 35 list the comparison of engine performance using Jet-A and LH_2 (three cases), at TOC (on-design point), SLS, cruise, climb and loiter points, respectively. Also, Table SI 31 provides comparison of combustion product species, mass, momentum, and total energy between LH_2 Case 1 and Jet-A engine at design point/TOC condition (same thrust production). Also, the values of thrust required mentioned in Tables SI 30, SI 32, and SI 33, are calculated through an iterative and interactive process between the proposed/present engine model and the aircraft weight sizing process. The process for thrust requirement calculations is discussed in detail, in [66].

It can be observed from Tables SI 30, SI 32, and SI 33 that the engine designs successfully meet the design requirements/targets as set in Table 3 and Table SI 4. In Tables Tables SI 30, SI 32, and SI 33, the engine designs meet the required thrust values for all three cases of LH_2 fuelled engine, at said mission points considered in these tables. These thrust requirements are calculated through the aircraft weight sizing process (details in [66]).

According to the study by Corchero et al. [67], T_4 in hydrogen-based gas turbine engines decreases by approximately to 37 K compared to Jet-A engines for same thrust production at SLS, which translates into a significantly longer engine life. As can be observed from Table SI 32, at SLS point, for same thrust production (case 1) the LH_2 engine operates at about 46 K lower T_4 compared to Jet-A engine. This is similar to the findings of Corchero et al. The reason for the reduction in T_4 is discussed below with the consideration of combustion chemistry.

When a fluid mass flows through a control volume, it is accompanied by its energy. These include four types of energy: internal energy, kinetic energy, potential energy, and flow work [68]. Therefore, any given fluid flow through a control volume is analysed by the mass, momentum, and total energy equations between the entry point and the exit point of the control volume.

Table SI 30. Comparison of engine performance at TOC condition using LH_2 fuel (three cases) and Jet-A, using the proposed model

TOC parameters	Units	Jet-A	LH_2		
			Case 1	Case 2	Case 3
Mach, altitude	- , m	0.8 at 10,668 m	0.8 at 10,668 m	0.8 at 10,668 m	0.8 at 10,668 m
Engine mass flow	kg/s	638.06	638.06	571.92	558.79
Thrust required	kN	55.603	46.29	46.02	45.66
Thrust produced	kN	55.603	55.603	46.354	46.12
TSFC	g/kN-s	12.399	4.328	4.284	4.160
TSEC	kJ/kN-s	535.67	519.36	514.06	499.14
TSEC % difference compared to Jet-A	%	-	-3.04	-4.03	-6.82
Fuel consumption	kg/s	0.689	0.241	0.199	0.192
Fuel-air ratio (FAR)	-	0.025191	8.7927E-3	8.0942E-3	6.4021E-3
Φ	-	0.37	0.30	0.28	0.22
OPR	-	60	60	60	60
BPR	-	17.65	17.65	17.65	17.65
FPR	-	1.35	1.35	1.35	1.35
IPC pressure ratio	-	3.296	3.296	3.296	3.296
HPC pressure ratio	-	13.9	13.9	13.9	13.9
Cooling flow	%	20	20	20	Zero
Combustor length	m	0.1981	0.1981	0.18723	0.18505
Combustion gas velocity	m/s	235.68	238.45	234.29	223.6
Residence time	ms	0.841	0.831	0.8	0.826
P_3	kPa	2,159.4	2,159.4	2,159.4	2,159.4
T_3	K	859.4	859.5	859.5	859.5
T_4	K	1,689.61	1,642.39	1588.50	1,452.50
T_4/T_2	-	6.844	6.653	6.434	5.883
Bare engine weight	kg	4,411	4,381	4,084	3,636
Gear ratio	-	3.5	3.5	3.11	3.11
Fan diameter	m	3.36296	3.36296	3.1839	3.14713
LPT inlet temperature	K	1,139	1,111	1,060	1,054
Power off-take	kW		150		

Table SI 31. Comparison of combustion product species, mass, momentum, and total energy between LH_2 Case 1 and Jet-A engine at TOC condition (same thrust production)

Baseline Jet-A FAR = 0.025191 (in equation SI 7), at TOC condition					
	CO_2	H_2O	O_2	N_2	Total
Molecular weight (kg/k-mol)	44	18	32	28	-
Number of moles	0.0522	0.0495	0.1330	0.7900	1.025
Mole fraction	0.0509	0.0483	0.1298	0.7709	1
Molar heat capacity C_p (J/mol-K)	3.5 R'	4 R'	3.5 R'	3.5 R'	-
Mass (kg)	2.297	0.892	4.257	22.131	*29.577*
Molar heat capacity C_p of combustion products (J/mol-K)					3.524 R'
Molecular weight of combustion products (kg/k-mol)					28.863
Mass flow rate at combustor exit (kg/s) [from GasTurb 13]					28.06
Time consumed by ~ *29.577 kg* of combustion products to flow (sec)					1.054
Fuel flow rate (kg/s) [from GasTurb 13]					0.689
Fuel mass combusted by one k-mol of air (kg) [using equation SI 7]					0.727
Time taken for the combustion of ~0.727 kg fuel (sec)					1.054
Total pressure at combustor exit (kPa) [from GasTurb 13]					2,073.06
Total enthalpy at combustor exit (MJ/kg) [from GasTurb 13]					1.63
Specific heat capacity c_p at total temperature at combustor exit (J/kg-K) [from GasTurb 13]					1,287.22
Emission index of H_2O (kg H_2O per kg fuel)					1.23
Case 1 H_2 FAR = 8.7927×10^{-3} (in equation SI 8), at TOC condition					
	CO_2	H_2O	O_2	N_2	Total
Molecular weight (kg/k-mol)	44	18	32	28	-
Number of moles	0	0.1258	0.1471	0.7900	1.063
Mole fraction	0	0.1184	0.1384	0.7432	1
Molar heat capacity C_p (J/mol-K)	-	4 R'	3.5 R'	3.5 R'	-
Mass (kg)	0	2.267	4.706	22.131	*29.104*
Molar heat capacity C_p of combustion products (J/mol-K)					3.559 R'
Molecular weight of combustion products (kg/k-mol)					27.381
Mass flow rate at combustor exit (kg/s) [from GasTurb 13]					27.611
Time consumed by ~ *29.104 kg* of combustion products to flow (sec)					1.054
Fuel flow rate (kg/s) [from GasTurb 13]					0.241
Fuel mass combusted by one k-mol of air (kg) [using equation SI 8]					0.254
Time taken for the combustion of ~0.254 kg fuel (sec)					1.054
Total pressure at combustor exit (kPa) [from GasTurb 13]					2,073.06
Total enthalpy at combustor exit (MJ/kg) [from GasTurb 13]					1.63
Specific heat capacity c_p at total temperature at combustor exit (J/kg-K) [from GasTurb 13]					1,343.13
Emission index of H_2O (kg H_2O per kg fuel)					8.937

* R' is the universal gas constant

Referring to Table SI 30 i.e., the design point/TOC, it can be observed that for same thrust production, the TSFC value of Jet-A is 2.865 times the TSFC value for LH_2 Case 1, whereas the energy density per unit mass of LH_2 is 2.78 times the energy density per unit mass of Jet-A. This (TSFC of LH_2 Case 1 vs Jet-A) can also be observed at off-design/other points in Table SI 32 – Table SI 35. This reduction in TSFC is attributable to difference in the combustion chemistry of the two fuels, in totality, which comprise of two effects: energy densities of two fuels, and mass and species conservation. Hydrogen burns much leaner than expected compared to Jet-A, for same thrust production at all mission points. Additionally, as described above, burner temperature (T_4) of Case 1 of LH_2 engine for same thrust production is about 47 K lower than that for Jet-A engine. Thus, for producing the same thrust, lower LH_2 fuel is required or hydrogen burns 'much leaner' than expected, compared to Jet-A.

The physics can further be understood through Table SI 31, which provides a comparison of combustion product species, mass, momentum, and total energy between LH_2 Case 1 and Jet-A engine at TOC condition (same thrust production). The mass of the product species is calculated using equations SI 7 and SI 8 (SI §1.3.1) for Jet-A and hydrogen respectively (with FAR for Jet-A and LH_2 Case 1 from Table SI 30). As discussed before in SI §1.3.1, these equations are based on a simplistic major species model. It can be observed that the mass of combustion products/gas for both Jet-A and LH_2 Case 1 is similar. This is despite the fact that hydrogen combustion does not produce any CO_2. Hence for achieving the same mass of combustion products/gas, which can impart same momentum on the turbines (for same thrust production), hydrogen burns much leaner than Jet-A. The extra air from the leaner combustion, especially oxygen, contribute to the mass requirement of the combustion product/gas. This can be observed from Table SI 31, where the mass of oxygen (heavier gas relative to air) in the combustion products of hydrogen combustion is greater than that for Jet-A combustion. Moreover, this extra oxygen also contributes to the formation of higher mass of water for hydrogen engine compared to Jet-A engine. This can be observed from Table SI 31, where the mass of water in the combustion products of hydrogen combustion is significantly greater than that for Jet-A combustion. In terms of emissions index (EI), the EI (H_2O) for Jet-A and LH_2 are calculated to be 1.23 kg/kg-fuel and 8.937 kg/kg-fuel, respectively. These calculated values are very similar to the EI reported in literature of 1.24 kg/kg-fuel [69] and 8.937 kg/kg-fuel [70] for Jet-A and LH_2, respectively.

Therefore, lean combustion of hydrogen enables the inclusion of more heavy gas molecules such that the mass of the combustion products is similar to the combustion products of Jet-A, and both cases thus result in similar momentum of combustion products. It can be observed from Table SI 31, that both Jet-A and LH_2 Case 1 engines have same total pressure at combustor exit. Pressure (static and dynamic) is a measure of the momentum. Lastly, both Jet-A and LH_2 Case 1 engines have same 'total enthalpy' (measure of energy) of 1.63 MJ/kg. Additionally, using equations SI 7 and SI 8, and GasTurb 13, it can be observed from Table SI 31 that both cases have: similar time scales for consumption of respective fuel mass with respective fuel consumption rate; and time taken by the mass of combustion products to flow with respective flow rate. Therefore, at the combustor exit point, both Jet-A and LH_2 Case 1 engines have similar mass, momentum, and energy, which enables both engines to produce same thrust. Thus, as observed from Table SI 30, for same thrust production, the TSFC value of Jet-A is 2.865 times the TSFC value for LH_2 Case 1. In summary, the ratio of energy density

per unit mass of LH_2 and Jet-A is 2.78 and it is a primary contributor to the above ratio of TSFC of 2.865 (ratio of TSFC of Jet-A and LH_2), and the difference in mass and species conservation in combustion chemical reaction of the two different fuels (discussed above) is the secondary contributor to this (2.865) ratio. According to the study by Verstraete [71], the drop in T_4 is also due to the increased heat capacity of combustion products of hydrogen for same thrust production. This aspect can also be observed in Table SI 31, where the specific heat capacity c_p of combustion products at total temperature of Case 1 of LH_2 engine is higher than Jet-A engine. The increase in the heat capacity can be understood from statistical mechanics. From statistical mechanics, the molar heat capacity is a measure of momentum/kinetic energy [72]. The molar heat capacity (J/mol-K) for an ideal gas, through equipartition principle can be represented by the translational, rotational, vibrational, and other modes of kinetic energy. For typical gas turbine operational temperatures (< 2,000 K), only translational and rotational energies are completely activated. According to equipartition principle, (the molar heat capacity at constant volume C_v), $C_{v,translational}$ is nR'/2 and $C_{v,rotational}$ is mR'/2, where n and m are translational and rotational degrees of freedom respectively, and R' is the universal gas constant. For an ideal gas, the molar heat capacity at constant pressure $C_P = R' + C_v$. For a linear molecule (CO_2, O_2, and N_2), there are three translational and two rotational modes/degrees of freedom (one redundant) i.e., $C_v = 2.5$ R' and $C_P = 3.5$ R', and for a non-linear molecule (H_2O), there are three translational and three rotational modes/degrees of freedom i.e., $C_v = 3$ R' and $C_P = 4$ R'. The molar C_p of the combustion products of Jet-A and Case 1 of LH_2 are calculated to be 3.524 R' and 3.559 R' respectively as listed in Table SI 31.

The above reasons are therefore responsible for the ~ 47 K drop in burner temperature (T_4) of Case 1 of LH_2 engine compared to Jet-A engine, for same thrust production. It is further observed that in the hydrogen engine for same thrust production, the T_4 is about 47 K lower than Jet-A engine, and this further reduces the FAR or hydrogen burns 'much leaner' than expected, and this is attributable to the difference in mass and species conservation of Jet-A and hydrogen (as discussed above).

The TSFC in Table SI 30, Table SI 32 – Table SI 35 is converted to thrust specific energy consumption (TSEC) by multiplying every case with the energy density of the respective fuel considered. The reduction in TSFC is attributable to difference in the combustion chemistry of the two fuels, in totality, which comprise of two effects: energy densities of two fuels, and mass and species conservation. As observed from Table SI 30, hydrogen engine (case 1) is 3% more energy efficient than Jet-A engine, for same thrust production.

Table SI 32. Comparison of engine performance at SLS condition using LH_2 fuel (three cases) and Jet-A, using the proposed model

SLS parameters	Units	Jet-A	LH_2		
			Case 1	Case 2	Case 3
Mach, altitude	- , m	0 at 0 m	0 at 0 m	0 at 0 m	0 at 0 m
Engine mass flow	kg/s	1,526.97	1,528.70	1,356.61	1,331.98
Thrust required	kN	299.9	251.1	249.6	247.7
Thrust produced	kN	303.9	304.5	263.8	261.1
TSFC	g/kN-s	5.124	1.778	1.761	1.690
TSEC	kJ/kN-s	221.37	213.34	211.34	202.78
TSEC % difference compared to Jet-A	%	-	-3.63	-4.53	-8.40
Fuel consumption	kg/s	1.557	0.541	0.465	0.441
FAR	-	0.026912	9.346E-3	9.0383E-3	6.9941E-3
Φ	-	0.39	0.32	0.31	0.24
OPR	-	47.1	47.1	47.1	47.1
BPR	-	20	20	20	20
FPR	-	1.25	1.25	1.25	1.25
IPC pressure ratio	-	3.028	3.044	2.890	2.945
HPC pressure ratio	-	12.769	12.702	13.391	13.031
Cooling flow	%	20	20	20	Zero
Combustor length	m	0.1981	0.1981	0.1872	0.1851
Combustion gas velocity	m/s	241.78	244.57	243.21	230.82
Residence time	ms	0.82	0.81	0.77	0.80
P_3	kPa	4,724.8	4,724.5	4,724.7	4,724.7
T_3	K	914	914	914	912
T_4	K	1,776	1,720	1,698	1,539
T_4/T_2	-	6.163	5.97	5.892	5.342
LPT inlet temperature	K	1,213	1,179	1,152	1,135
Power off-take	kW		150		

Additionally, it can be observed from Table SI 30, Table SI 32 – Table SI 35 that all three cases of LH_2 engine operate at a lower T_4 compared to the Jet-A engine. Especially, for case 1 of LH_2 engine i.e., for similar thrust production, the T_4 is lower (as described above) compared Jet-A engine because H_2 burns much leaner than Jet-A. Additionally, it can be observed from Table SI 30, Table SI 32 – Table SI 35 that the thrust values drop between Case 1 and Case 3 of LH_2, because the effect of lighter LH_2 aircraft weight is considered. Therefore, T_4 drops between Case 1 and Case 3 of LH_2, which is expected. In Case 3 of LH_2, there are no cooling flows (at on-design and all four off-design points) because the engine is operating at significantly lower T_4 (approximate reduction of 200 K) and the design decision to consider this case specifically in the study, is well supported. Because there are no cooling flows, the engine must consume less fuel compared to Case 2 of LH_2. The drop in thrust values as discussed above for Table SI 30, Table SI 32 – Table SI 35, along with the effect of zero cooling

flows in Case 3 of LH_2, both are attributable to the TSFC drop between Case 1 and Case 3 of LH_2. Overall, these above discussed effects (lower FAR or lower T_4, lighter aircraft, and reduction in cooling flows) result in the reduction of TSEC from LH_2 Case 1 (3%) to Case 3 (6.82%), compared to Jet-A engine, which can be observed from Table SI 30, Table SI 32 – Table SI 35.

As observed from Table SI 30, the engine weight of Case 1 of LH_2 is lower than Jet-A engine by approximately 30 kg for same thrust production despite both cases having same stage counts of turbomachinery and same advanced materials. This is primarily attributable to lower T_4 (-47 K) of LH_2 Case 1, which results in lower aero-thermal and mechanical loading of LPT section in GasTurb 13. In other words, Jet-A engine has higher T_4 compared to LH_2 Case 1. Therefore, the LPT section loading of Jet-A engine is slightly higher than LH_2 Case 1, which results in ~ 30 kg higher weight. It is to be noted that the LPT inlet temperatures at all points (on-design and off-design) in engine designs listed in Table SI 30, Table SI 32 – Table SI 35, are lower than 1,350 K which was required for having uncooled LPT. This design choice was successful primarily because of the use of future component efficiencies.

Table SI 33. Comparison of engine performance at cruise condition using LH_2 fuel (three cases) and Jet-A, using the proposed model

Cruise parameters	Units	Jet-A	LH_2		
			Case 1	Case 2	Case 3
Mach, altitude	- , m	0.84 at 10,668 m	0.84 at 10,668 m	0.84 at 10,668 m	0.84 at 10,668 m
Engine mass flow	kg/s	649.7	649.8	602.9	569.7
Thrust required	kN	42.25	40.24	40.15	40.02
Thrust produced	kN	51.61	51.68	51.09	43.12
TSFC	g/kN-s	12.667	4.424	4.351	4.278
TSEC	kJ/kN-s	547.2	530.9	522.1	513.4
TSEC % difference compared to Jet-A	%	-	-2.98	-4.59	-6.16
Fuel consumption	kg/s	0.654	0.229	0.222	0.185
FAR	-	0.024099	8.4241E-3	7.9129E-3	6.0565E-3
Φ	-	0.35	0.29	0.27	0.21
Combustor length	m	0.1981	0.1981	0.1872	0.1851
Combustion gas velocity	m/s	231.99	234.68	234.00	219.89
Residence time	ms	0.854	0.842	0.801	0.842
P_3	kPa	2,108.29	2,110.35	2,473.61	2,162.54
T_3	K	838	838	876	843
T_4	K	1,640	1,597	1,588	1,410
T_4/T_2	-	6.567	6.394	6.359	5.645
Cooling flow	%	20	20	20	Zero
LPT inlet temperature	K	1,107	1,081	1,066	1,025
Power off-take	kW	150			

Table SI 34. Comparison of engine performance at climb condition using LH_2 fuel (three cases) and Jet-A, using the proposed model

Climb parameters	Units	Jet-A	LH_2		
			Case 1	Case 2	Case 3
Mach, altitude	- , m	0.47 at 5334 m	0.47 at 5,334 m	0.47 at 5,334 m	0.47 at 5,334 m
Engine mass flow	kg/s	904.96	906.71	857.06	798.62
Thrust produced	kN	94.94	95.54	96.96	82.58
TSFC	g/kN-s	9.798	3.413	3.389	3.266
TSEC	kJ/kN-s	423.26	409.58	406.73	391.91
TSEC % difference compared to Jet-A	%	-	-3.23	-3.91	-7.41
Fuel consumption	kg/s	0.930	0.326	0.329	0.270
FAR	-	0.024524	8.5724E-3	8.0763E-3	6.2803E-3
Φ	-	0.36	0.29	0.28	0.21
Combustor length	m	0.1981	0.1981	0.1872	0.1851
Combustion gas velocity	m/s	234.28	237.10	237.14	223.33
Residence time	ms	0.846	0.836	0.79	0.829
P_3	kPa	2,978.50	2,989.01	3,632.44	3,093.35
T_3	K	861	862	910	868
T_4	K	1672	1628	1628	1450
T_4/T_2	-	6.315	6.149	6.152	5.478
Cooling flow	%	20	20	20	Zero
LPT inlet temperature	K	1,129	1,102	1,096	1,054
Power off-take	kW		150		

Table SI 35. Comparison of engine performance at loiter condition using LH_2 fuel (three cases) and Jet-A, using the proposed model

Loiter parameters	Units	Jet-A	LH_2		
			Case 1	Case 2	Case 3
Mach, altitude	- , m	0.6 at 1500 m	0.6 at 1500 m	0.6 at 1500 m	0.6 at 1500 m
Engine mass flow	kg/s	1,488.32	1,490.63	1,403.87	1,307.75
Thrust produced	kN	114.67	115.46	120.05	98.02
TSFC	g/kN-s	12.175	4.234	4.195	4.067
TSEC	kJ/kN-s	525.94	508.03	503.35	487.98
TSEC % difference compared to Jet-A	%	-	-3.41	-4.30	-7.22
Fuel consumption	kg/s	1.397	0.489	0.504	0.399
FAR	-	0.024892	8.6933E-3	8.0066E-3	6.3186E-3
Φ	-	0.36	0.30	0.27	0.22
Combustor length	m	0.1981	0.1981	0.1872	0.1851
Combustion gas velocity	m/s	237.44	240.26	239.83	226.44
Residence time	ms	0.835	0.825	0.781	0.818
P_3	kPa	4,486.2	4,499.9	5,715.1	4,624.2
T_3	K	905	906	967	911
T_4	K	1,713	1,667	1,665	1,486
T_4/T_2	-	5.741	5.586	5.579	4.977
Cooling flow	%	20	20	20	Zero
LPT inlet temperature	K	1,167	1,139	1,133	1,087
Power off-take	kW		150		

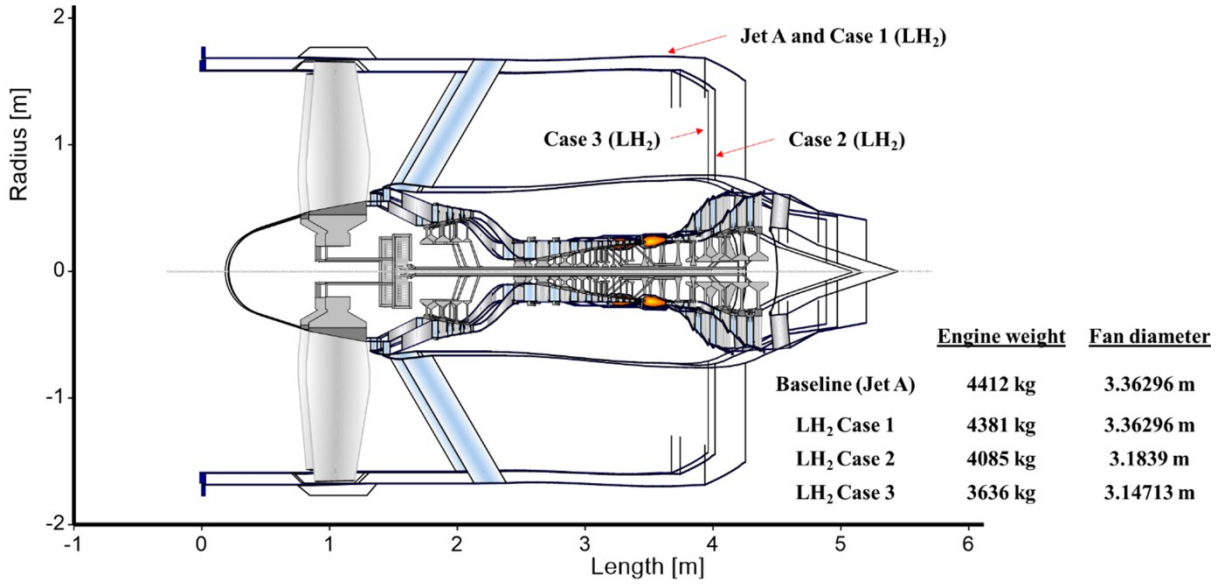

Figure SI 9. Cross-sectional view of the Jet-A powered GTF engine overlapped with the three cases of LH_2 powered GTF engine designed using the proposed model

SI 5.4 Trend of engine technology development

Table SI 36. Different efficiency metrics during cruise for engines entered in service till date (data source [73]) and engines modelled in this work

Aircraft	Effective propulsive efficiency	Core efficiency	Overall efficiency
B707	0.485	0.440	0.213
B727	0.585	0.440	0.257
MD80	0.615	0.450	0.277
B747-100	0.625	0.480	0.300
A300	0.650	0.500	0.325
B757	0.665	0.510	0.339
B747-400	0.680	0.500	0.340
B777	0.700	0.530	0.371
B787	0.715	0.550	0.393
A380	0.690	0.570	0.393
A350	0.710	0.563	0.400
Propfan	0.760	0.526	0.455
BWB UHB GTF Jet-A	0.752	0.605	0.469
BWB UHB GTF 100% SPK	0.752	0.605	0.477
BWB UHB GTF LH2 C1	0.750	0.626	0.485
BWB UHB GTF LH2 C2	0.756	0.631	0.455
BWB UHB GTF LH2 C3	0.756	0.641	0.400

More information:

First author's other research work can be found in [31], [66], [74]–[102].

References

[1] D. Raymer, *Aircraft Design: A Conceptual Approach, Sixth Edition*. Washington, DC: American Institute of Aeronautics and Astronautics, Inc., 2018. doi: 10.2514/4.104909.

[2] M. H. Sadraey, *Aircraft Design: A Systems Engineering Approach*. John Wiley and Sons, 2012. doi: 10.1002/9781118352700.

[3] J. P. Fielding, *Introduction to Aircraft Design*. Cambridge University Press, 2017. doi: 10.1017/9781139542418.

[4] M. R. Kirby, "A methodology for technology identification, evaluation, and selection in conceptual and preliminary aircraft design," Georgia Institute of Technology, 2001. Accessed: Dec. 17, 2019. [Online]. Available: https://pdfs.semanticscholar.org/3e8f/f5be8491a4f30f4dbb9edce1ff08cfd5b45a.pdf

[5] E. Torenbeek, *Advanced Aircraft Design: Conceptual Design, Analysis and Optimization of Subsonic Civil Airplanes*. John Wiley and Sons, 2013. doi: 10.1002/9781118568101.

[6] A. K. Kundu, M. A. Price, and D. Riordan, *Conceptual Aircraft Design : an Industrial Perspective.*, First. John Wiley & Sons, Incorporated, 2019.

[7] E. S. Hendricks, "A multi-level multi-design point approach for gas turbine cycle and turbine conceptual design," Georgia Institute of Technology, 2017. Accessed: Oct. 17, 2019. [Online]. Available: https://smartech.gatech.edu/handle/1853/58212

[8] J. D. Mattingly, W. H. Heiser, and D. T. Pratt, *Aircraft Engine Design, Third Edition*. American Institute of Aeronautics and Astronautics, 2018. doi: https://doi.org/10.2514/4.105173.

[9] P. P. Walsh and P. Fletcher, *Gas Turbine Performance*. Wiley, 2004. doi: 10.1002/9780470774533.

[10] H. I. H. Saravanamuttoo, G. F. C. Rogers, H. Cohen, P. V. Straznicky, and A. C. Nix, *Gas Turbine Theory*, Seventh. Pearson, 2017. Accessed: Dec. 17, 2019. [Online]. Available: https://www.pearson.com/us/higher-education/program/Cohen-Gas-Turbine-Theory-7th-Edition/PGM1943364.html

[11] H. Nojoumi, I. Dincer, and G. F. Naterer, "Greenhouse gas emissions assessment of hydrogen and kerosene-fueled aircraft propulsion," *Int. J. Hydrogen Energy*, vol. 34, no. 3, pp. 1363–1369, Feb. 2009, doi: 10.1016/J.IJHYDENE.2008.11.017.

[12] S. R. Turns, *An introduction to combustion : concepts and applications*. McGraw-Hill, 2012.

[13] C. Marek, T. Smith, and K. Kundu, "Low Emission Hydrogen Combustors for Gas Turbines Using Lean Direct Injection," in *41st AIAA/ASME/SAE/ASEE Joint Propulsion Conference & Exhibit*, Jul. 2005. doi: 10.2514/6.2005-3776.

[14] "Table of gaseous composition of dry air." https://eesc.columbia.edu/courses/ees/slides/climate/table_1.html (accessed Jan. 15, 2020).

[15] D. N. Anderson, "EMISSIONS OF OXIDES OF NITROGEN FROM AN

EXPERIMENTAL PREMIXED-HYDROGEN BURNER," Cleveland, Ohio, 1976. Accessed: Jan. 15, 2020. [Online]. Available: https://ntrs.nasa.gov/search.jsp?R=19760016183

[16] N. A. Cumpsty, *Jet propulsion : a simple guide to the aerodynamics and thermodynamic design and performance of jet engines*. 2015.

[17] J. Kurzke, "GasTurb 13," *GasTurb GmbH*, 2017. https://gasturb.de/software/gasturb.html

[18] P. Dagaut and M. Cathonnet, "The ignition, oxidation, and combustion of kerosene: A review of experimental and kinetic modeling," *Progress in Energy and Combustion Science*, vol. 32, no. 1. pp. 48–92, 2006. doi: 10.1016/j.pecs.2005.10.003.

[19] D. J. Poferl and R. A. Svehla, "THERMODYNAMIC AND TRANSPORT PROPERTIES OF AIR AND ITS PRODUCTS OF COMBUSTION WITH ASTM-A-1 FUEL AND NATURAL GAS," 1973. Accessed: Jan. 15, 2020. [Online]. Available: https://ntrs.nasa.gov/search.jsp?R=19740004462

[20] W. G. Vincenti and C. H. Kruger, *Introduction to physical gas dynamics*. Krieger, 1975.

[21] C. Vallance, *An Introduction to Chemical Kinetics*. IOP Publishing, 2017. doi: 10.1088/978-1-6817-4664-7.

[22] J. Seitzman, "Laminar Flame Speed," 2004. http://seitzman.gatech.edu/classes/ae6766/PremixedLaminarFlames.pdf (accessed Jan. 11, 2020).

[23] J. Seitzman, "Premixed Flames: Propagation Limits and Stability," 2004. http://seitzman.gatech.edu/classes/ae6766/FlamePropagationLimits.pdf (accessed Jan. 11, 2020).

[24] B. Khandelwal, A. Karakurt, P. R. Sekaran, V. Sethi, and R. Singh, "Hydrogen powered aircraft: The future of air transport," *Progress in Aerospace Sciences*, vol. 60. Elsevier Ltd, pp. 45–59, 2013. doi: 10.1016/j.paerosci.2012.12.002.

[25] G. L. Juste, "Hydrogen injection as additional fuel in gas turbine combustor. Evaluation of effects," *Int. J. Hydrogen Energy*, vol. 31, no. 14, pp. 2112–2121, Nov. 2006, doi: 10.1016/j.ijhydene.2006.02.006.

[26] G. Dahl and F. Suttrop, "Engine control and low-nox combustion for hydrogen fuelled aircraft gas turbines," *Int. J. Hydrogen Energy*, vol. 23, no. 8, pp. 695–704, Aug. 1998, doi: 10.1016/s0360-3199(97)00115-8.

[27] "GasTurb - GasTurb." https://gasturb.de/software/gasturb.html (accessed Apr. 10, 2020).

[28] J. Kurzke, "GasTurb 13 Design and Off-Design Performance of Gas Turbines," 2018.

[29] J. Kurzke and I. Halliwell, *Propulsion and Power: An Exploration of Gas Turbine Performance Modeling*. Springer International Publishing, 2018. doi: 10.1007/978-3-319-75979-1.

[30] C. L. Nickol and W. J. Haller, "Assessment of the Performance Potential of Advanced Subsonic Transport Concepts for NASA's Environmentally Responsible Aviation

Project," in *54th AIAA Aerospace Sciences Meeting*, Jan. 2016. doi: 10.2514/6.2016-1030.

[31] S. S. Jagtap, P. R. N. Childs, and M. E. J. Stettler, "Energy performance evaluation of alternative energy vectors for subsonic long-range tube-wing aircraft," *Transp. Res. Part D Transp. Environ.*, vol. 115, p. 103588, Feb. 2023, doi: 10.1016/J.TRD.2022.103588.

[32] E. M. Greitzer *et al.*, "N+3 Aircraft Concept Designs and Trade Studies, Final Report, Volume 1," 2010. [Online]. Available: https://ntrs.nasa.gov/archive/nasa/casi.ntrs.nasa.gov/20100042401.pdf

[33] B. K. Kestner, J. S. Schutte, J. C. Gladin, and D. N. Mavris, "Ultra high bypass ratio engine sizing and cycle selection study for a subsonic commercial aircraft in the N+2 timeframe," in *Proceedings of the ASME Turbo Expo*, 2011, vol. 1, pp. 127–137. doi: 10.1115/GT2011-45370.

[34] Bijewitz J, Seitz A, and M. Hornung, "Architectural Comparison of Advanced Ultra-High Bypass Ratio Turbofans for Medium to Long Range Application," in *Deutscher Luft- und Raumfahrtkongress 2014*, 2014.

[35] M. A. Engines, "PW1100G-JM engine." https://www.mtu.de/maintenance/commercial-aircraft-engine-services/engine-portfolio-mro/narrowbody-and-regional-jets/pw1100g-jm/ (accessed Dec. 20, 2019).

[36] S. Liu and Y. C. Shin, "Additive manufacturing of Ti6Al4V alloy: A review," *Mater. Des.*, vol. 164, Feb. 2019, doi: 10.1016/j.matdes.2018.107552.

[37] S. C. Joshi and A. A. Sheikh, "3D printing in aerospace and its long-term sustainability," *Virtual Phys. Prototyp.*, vol. 10, no. 4, pp. 175–185, Oct. 2015, doi: 10.1080/17452759.2015.1111519.

[38] "Damage-Tolerant Fan Casings for Jet Engines." https://spinoff.nasa.gov/Spinoff2006/T_1.html (accessed Dec. 04, 2019).

[39] L. Liu *et al.*, "Ballistic impact testing and analysis of triaxial braided composite fan case material," in *Advanced Materials Research*, 2012, vol. 535–537, pp. 121–132. doi: 10.4028/www.scientific.net/AMR.535-537.121.

[40] R. Coroneos, "Structural Analysis and Optimization of a Composite Fan Blade for Future Aircraft Engine," 2012. Accessed: Dec. 04, 2019. [Online]. Available: https://ntrs.nasa.gov/archive/nasa/casi.ntrs.nasa.gov/20120013597.pdf

[41] J. A. Dicarlo, "Advances in SiC/SiC Composites for Aero-Propulsion," 2013. Accessed: Dec. 04, 2019. [Online]. Available: http://www.sti.nasa.gov

[42] T. Hinoki, E. Lara-Curzio, and L. L. Snead, "Mechanical properties of high purity SiC fiber-reinforced CVI-SiC matrix composites," *Fusion Sci. Technol.*, vol. 44, no. 1, pp. 211–218, 2003, doi: 10.13182/FST03-A336.

[43] "Tyranno Fiber® - UBE INDUSTRIES,LTD." https://www.ube.com/contents/en/chemical/continuous_inorganic_fiber/tyranno_fiber.html#h2_id_2 (accessed Dec. 04, 2019).

[44] I. Spitsberg and J. Steibel, "Thermal and Environmental Barrier Coatings for SiC/SiC CMCs in Aircraft Engine Applications*," *Int. J. Appl. Ceram. Technol.*, vol. 1, no. 4,

pp. 291–301, Jan. 2005, doi: 10.1111/j.1744-7402.2004.tb00181.x.

[45] M. Wilkie and M. Lucas, “The effect of Ti-6Al-4V microstructure on the performance of ultrasonic soft tissue cutting tips,” *Cit. Proc. Mtgs. Acoust*, vol. 32, p. 20010, 2017, doi: 10.1121/2.0000735.

[46] “Titanium Alloys for Aeroengine and Airframe Applications.” https://www.azom.com/article.aspx?ArticleID=1569 (accessed Dec. 04, 2019).

[47] I. Inagaki, T. Takechi, Y. Shirai, and N. Ariyasu, “Application and Features of Titanium for the Aerospace Industry,” 2014. Accessed: Dec. 04, 2019. [Online]. Available: https://www.nipponsteel.com/en/tech/report/nssmc/pdf/106-05.pdf

[48] United-Performance-Metals, “Properties of Nickel Alloy 718.” https://www.upmet.com/sites/default/files/datasheets/718.pdf (accessed Dec. 04, 2019).

[49] F. Yin and A. Gangoli Rao, “Performance analysis of an aero engine with inter-stage turbine burner,” in *Aeronautical Journal*, Nov. 2017, vol. 121, no. 1245, pp. 1605–1626. doi: 10.1017/aer.2017.93.

[50] I. Halliwell, “An Ultra-High Bypass Ratio Turbofan Engine for the Future,” 2014. https://pdfslide.us/documents/undergraduate-team-engine-student-design-competition-2014-undergraduate.html (accessed Dec. 09, 2019).

[51] J. Li, X. Sun, Y. Liu, and V. Sethi, “Preliminary Aerodynamic Design Methodology for Aero Engine Lean Direct Injection Combustors,” *Aeronaut. J.*, vol. 121, pp. 1087–1108, 2017, doi: 10.1017/aer.2017.47.

[52] “Pratt and Whitney PW1100G Geared Turbofan Engine | The Flying Engineer.” http://theflyingengineer.com/flightdeck/pw1100g-gtf/ (accessed Dec. 06, 2019).

[53] Skybrary, “BOEING 787-8 Dreamliner - SKYbrary Aviation Safety.” https://www.skybrary.aero/index.php/B788 (accessed Dec. 07, 2019).

[54] Skybrary, “AIRBUS A350-900 - SKYbrary Aviation Safety.” https://www.skybrary.aero/index.php/A359 (accessed Dec. 07, 2019).

[55] A. R. A. Talib, E. Gires, and M. T. Ahmad, “Performance Evaluation of a Small-Scale Turbojet Engine Running on Palm Oil Biodiesel Blends,” 2014, doi: 10.1155/2014/946485.

[56] E. G. Tulapurkara, A. Venkattraman, and V. Ganesh, “AN EXAMPLE OF AIRPLANE PRELIMINARY DESIGN PROCEDURE-JET TRANSPORT,” 2007. https://nptel.ac.in/content/storage2/courses/101106035/057_Appendix 10.2_(05-10-2013).pdf (accessed Dec. 07, 2019).

[57] Society-of-Robots, “High Altitude Balloon Tutorial: Measuring Humidity.” https://www.societyofrobots.com/space_balloon_humidity_test.shtml (accessed Dec. 07, 2019).

[58] H. Gazzetta Junior, C. Bringhenti, J. Roberto Barbosa, and J. T. Tomita, “Real-Time Gas Turbine Model for Performance Simulations,” *J. Aerosp. Technol. Manag. São José dos Campos*, vol. 9, no. 3, pp. 346–356, doi: 10.5028/jatm.v9i3.693.

[59] J. Bijewitz, A. Seitz, A. T. Isikveren, and M. Hornung, “Multi-disciplinary design

investigation of propulsive fuselage aircraft concepts," *Aircr. Eng. Aerosp. Technol.*, vol. 88, no. 2, pp. 257–267, Mar. 2016, doi: 10.1108/AEAT-02-2015-0053.

[60] ANL, "GREET 2021," *Argonne National Laboratory*, 2021. https://greet.es.anl.gov/

[61] E. Gamble, D. Terrell, and R. DeFrancesco, "Nozzle Selection and Design Criteria," Jul. 2004. doi: 10.2514/6.2004-3923.

[62] A. Manneville, "Propulsion System Concepts for Silent Aircraft," MIT, 2004. Accessed: Dec. 06, 2019. [Online]. Available: https://core.ac.uk/download/pdf/4385607.pdf

[63] J. W. Chapman, T. M. Lavelle, and J. S. Litt, "Practical Techniques for Modeling Gas Turbine Engine Performance." Accessed: Dec. 07, 2019. [Online]. Available: https://ntrs.nasa.gov/search.jsp?R=20170000884

[64] B. Roth and J. de Luis, "LOST THRUST METHODOLOGY FOR GAS TURBINE ENGINE PERFORMANCE ANALYSIS," in *ASME Turbo Expo 2005*, 2005. Accessed: Dec. 07, 2019. [Online]. Available: https://smartech.gatech.edu/bitstream/handle/1853/10606/GT-2005-68200.pdf

[65] A. Dankanich and D. Peters, "Turbofan Engine Bypass Ratio as a Function of Thrust and Fuel Turbofan Engine Bypass Ratio as a Function of Thrust and Fuel Flow Flow," 2017. Accessed: Dec. 07, 2019. [Online]. Available: https://openscholarship.wustl.edu/mems500https://openscholarship.wustl.edu/mems500/34

[66] S. S. Jagtap, P. R. N. Childs, and M. E. J. Stettler, "Conceptual design-optimisation of a subsonic hydrogen-powered long-range blended-wing-body aircraft," *Int. J. Hydrogen Energy*, vol. 96, pp. 639–651, Dec. 2024, doi: 10.1016/J.IJHYDENE.2024.11.331.

[67] G. Corchero and J. L. Montañ, "An approach to the use of hydrogen for commercial aircraft engines," *Proc. Inst. Mech. Eng. Part G J. Aerosp. Eng.*, vol. 219, no. 1, pp. 35–44, 2005, doi: 10.1243/095441005X9139.

[68] "First Law - Control Volumes - Energy Equation," *Ohio University website*, 2009. https://www.ohio.edu/mechanical/thermo/Intro/Chapt.1_6/Chapter4a.html (accessed Jan. 08, 2020).

[69] D. Wu, "Models, Optimal Performances and Sensitivities of Commercial Flight Trajectory in the Air Traffic System," UNIVERSITY OF MINNESOTA, 2012. Accessed: Jun. 10, 2022. [Online]. Available: https://conservancy.umn.edu/bitstream/handle/11299/144391/Wu_umn_0130E_13330.pdf?sequence=1&isAllowed=y

[70] M. Oak, A. Fabre, M. Delavenne, E. N. Van, E. Benard, and S. Defoort, "Spectral project - application of FAST-OAD code to the conceptual design of a hydrogen fuelled commercial aircraft," *IOP Conf. Ser. Mater. Sci. Eng.*, vol. 1226, no. 1, p. 012027, Feb. 2022, doi: 10.1088/1757-899X/1226/1/012027.

[71] D. Verstraete, "Long range transport aircraft using hydrogen fuel," *Int. J. Hydrogen Energy*, vol. 38, no. 34, pp. 14824–14831, Nov. 2013, doi: 10.1016/j.ijhydene.2013.09.021.

[72] S. J. Ling, W. Moebs, and J. Sanny, "Heat Capacity and Equipartition of Energy."

OpenStax, Sep. 15, 2016.

[73] National-Academies-of-Sciences-Engineering-and-Medicine, *Commercial Aircraft Propulsion and Energy Systems Research*. Washington, D.C.: National Academies Press, 2016. doi: 10.17226/23490.

[74] S. S. Jagtap, "Comparative assessment of manufacturing setups for blended sugar-to-aviation fuel production from non-food feedstocks for green aviation," in *AIAA Propulsion and Energy 2019 Forum*, 2019. doi: 10.2514/6.2019-4332.

[75] S. S. Jagtap, "A heat recovery system designed for shaft-powered aircraft gas turbine engines," 2016

[76] B. L. Emerson, S. Jagtap, and T. C. Lieuwen, "Stability Analysis of Reacting Wakes: Flow and Density Asymmetry Effects," in *53rd AIAA Aerospace Sciences Meeting*, Jan. 2015. doi: 10.2514/6.2015-0429.

[77] S. S. Jagtap, "Systems evaluation of subsonic hybrid-electric propulsion concepts for NASA N+3 goals and conceptual aircraft sizing," *Int. J. Automot. Mech. Eng.*, vol. 16, no. 4, pp. 7259–7286, 2019, doi: https://doi.org/10.15282/ijame.16.4.2019.07.0541.

[78] S. S. Jagtap, "A heat recovery system for shaft-driven aircraft gas turbine engines," Oct. 29, 2014

[79] S. S. Jagtap, "Assessment of feedstocks for blended alcohol-to-jet fuel manufacturing from standalone and distributed scheme for sustainable aviation," in *AIAA Propulsion and Energy 2019 Forum*, 2019. doi: 10.2514/6.2019-3887.

[80] S. S. Jagtap, "Evaluation of blended Fischer-Tropsch jet fuel feedstocks for minimizing human and environmental health impacts of aviation," in *AIAA Propulsion and Energy 2019 Forum*, 2019. doi: 10.2514/6.2019-4412.

[81] S. S. Jagtap, "Evaluation of technology and energy vector combinations for decarbonising future subsonic long-range aircraft," Imperial College London.

[82] S. S. Jagtap, M. E. J. Stettler, and P. R. N. Childs, "Data in brief: Performance sensitivity of subsonic liquid hydrogen long-range tube-wing aircraft to technology developments".

[83] S. S. Jagtap, M. E. J. Stettler, and P. R. N. Childs, "Data in brief: Conceptual design-optimisation of futuristic hydrogen powered ultrahigh bypass ratio geared turbofan engine".

[84] S. S. Jagtap, P. R. N. Childs, and M. E. J. Stettler, "Performance sensitivity of subsonic liquid hydrogen long-range tube-wing aircraft to technology developments," *Int. J. Hydrogen Energy*, vol. 50, pp. 820–833, Jan. 2024, doi: 10.1016/J.IJHYDENE.2023.07.297.

[85] S. S. Jagtap, M. E. J. Stettler, and P. R. N. Childs, "Data in brief: Conceptual design-optimisation of a subsonic hydrogen-powered long-range blended-wing-body aircraft".

[86] S. S. Jagtap, "Aero-thermodynamic analysis of space shuttle vehicle at re-entry," *IEEE Aerosp. Conf. Proc.*, vol. 2015-June, Jun. 2015, doi: 10.1109/AERO.2015.7119253.

[87] S. Jagtap and S. Bhandari, "Solar Refrigeration," *Sardar Patel Int. Conf.*, 2012, [Online]. Available: https://papers.ssrn.com/sol3/papers.cfm?abstract_id=2103115

[88] S. Jagtap and S. Bhandari, “Solar Refrigeration using Triple Fluid Vapor Absorption Refrigeration and Organic Rankine Cycle,” in *Sardar Patel International Conference SPICON 2012 Mechanical*, 2012.

[89] N. Komerath, S. Jagtap, and N. Hiremath, “Aerothermoelastic Tailoring for Waveriders,” in *US Air Force Summer Faculty Fellowship Program*, 2014.

[90] S. S. Jagtap, “Exploration of sustainable aviation technologies and alternative fuels for future inter-continental passenger aircraft.”

[91] S. S. Jagtap, “Identification of sustainable technology and energy vector combinations for future inter-continental passenger aircraft.”

[92] S. S. Jagtap, “Heat recuperation system for the family of shaft powered aircraft gas turbine engines,” US10358976B2, 2019 [Online]. Available: https://patents.google.com/patent/US10358976B2/en

[93] S. S. Jagtap, “Heat recovery system for shaft powered aircraft gas turbine engines”.

[94] S. S. Jagtap and S. Bhandari, “Systems design and experimental study of a solar parabolic trough for solar refrigeration”.

[95] S. S. Jagtap, “An Apparatus for Exchanging Heat with Flow in an Annulus,” *J. Eng. Sci. Technol. Rev.*, vol. 10, no. 1, pp. 173–176, 2017, Accessed: Jan. 11, 2019. [Online]. Available: http://www.jestr.org/downloads/Volume10Issue1/fulltext241012017.pdf

[96] S. S. Jagtap, “Conceptual aircraft sizing using systems engineering for N+3 subsonic hybrid-electric propulsion concepts”.

[97] S. S. Jagtap, P. R. N. Childs, and M. E. J. Stettler, “Conceptual design-optimisation of a future hydrogen-powered ultrahigh bypass ratio geared turbofan engine,” *Int. J. Hydrogen Energy*, vol. 95, pp. 317–328, Dec. 2024, doi: 10.1016/J.IJHYDENE.2024.10.329.

[98] S. S. Jagtap, M. E. J. Stettler, and P. R. N. Childs, “Data in brief: Energy performance evaluation of alternative energy vectors for subsonic intercontinental tube-wing aircraft”.

[99] S. Jagtap, A. Strehlow, M. Reitz, S. Kestler, and G. Cinar, “Model-Based Systems Engineering Approach for a Systematic Design of Aircraft Engine Inlet,” in *AIAA SCITECH 2025 Forum*, 2025. doi: https://doi.org/10.2514/6.2025-1410.

[100] S. S. Jagtap, “Non-food feedstocks comparison for renewable aviation fuel production towards environmentally and socially responsible aviation,” in *2019 AIAA Propulsion & Energy Forum*, 2019.

[101] B. Emerson, S. Jagtap, J. M. Quinlan, M. W. Renfro, B. M. Cetegen, and T. Lieuwen, “Spatio-temporal linear stability analysis of stratified planar wakes: Velocity and density asymmetry effects,” *Phys. Fluids*, vol. 28, no. 4, p. 045101, Apr. 2016, doi: 10.1063/1.4943238.

[102] S. S. Jagtap, “Sustainability assessment of hydro-processed renewable jet fuel from algae from market-entry year 2020: Use in passenger aircrafts,” in *16th AIAA Aviation Technology, Integration, and Operations Conference*, Jun. 2016. doi: 10.2514/6.2016-4367.